LETTER

https://doi.org/10.1038/s41586-018-0821-8

SETD3 is an actin histidine methyltransferase that prevents primary dystocia

Alex W. Wilkinson[1,9], Jonathan Diep[2,9], Shaobo Dai[3,9], Shuo Liu[1], Yaw Shin Ooi[2], Dan Song[4], Tie-Mei Li[1], John R. Horton[3], Xing Zhang[3], Chao Liu[4], Darshan V. Trivedi[4], Katherine M. Ruppel[4], José G. Vilches-Moure[5], Kerriann M. Casey[5], Justin Mak[6], Tina Cowan[7], Joshua E. Elias[8], Claude M. Nagamine[5], James A. Spudich[4], Xiaodong Cheng[3,10]*, Jan E. Carette[2,10]* & Or Gozani[1,10]*

For more than 50 years, the methylation of mammalian actin at histidine 73 has been known to occur[1]. Despite the pervasiveness of His73 methylation, which we find is conserved in several model animals and plants, its function remains unclear and the enzyme that generates this modification is unknown. Here we identify SET domain protein 3 (SETD3) as the physiological actin His73 methyltransferase. Structural studies reveal that an extensive network of interactions clamps the actin peptide onto the surface of SETD3 to orient His73 correctly within the catalytic pocket and to facilitate methyl transfer. His73 methylation reduces the nucleotide-exchange rate on actin monomers and modestly accelerates the assembly of actin filaments. Mice that lack SETD3 show complete loss of actin His73 methylation in several tissues, and quantitative proteomics analysis shows that actin His73 methylation is the only detectable physiological substrate of SETD3. SETD3-deficient female mice have severely decreased litter sizes owing to primary maternal dystocia that is refractory to ecbolic induction agents. Furthermore, depletion of SETD3 impairs signal-induced contraction in primary human uterine smooth muscle cells. Together, our results identify a mammalian histidine methyltransferase and uncover a pivotal role for SETD3 and actin His73 methylation in the regulation of smooth muscle contractility. Our data also support the broader hypothesis that protein histidine methylation acts as a common regulatory mechanism.

SETD3, a ubiquitously expressed protein, is epigenetically upregulated in response to muscle loading and hypertrophy[2]. SETD3 contains an N-terminal SET domain and a C-terminal domain that is homologous to a Rubisco large subunit methyltransferase (LSMT) interaction domain (Extended Data Fig. 1a). Proteins that contain a catalytic lysine methyltransferase SET domain are found in all three kingdoms of life and regulate diverse biological and pathological processes[3]. In humans, around half of the 55 SET family members methylate lysines on histone and/or non-histone protein substrates[3]. The enzymatic activities of the remainder of human SET proteins, including SETD3, are unclear. SETD3 has been reported to methylate histone H3 at lysines 4 and 36[4]. However, this conclusion was based on mass spectrometry data for which mass shifts were inconsistent with a bona fide methylation event (see figure 2c of a previous study[4]). When we tested the activity of SETD3, it did not methylate histones in contrast to two established protein lysine methyltransferases (PKMTs), NSD2 and MLL2[3] (Fig. 1a and Extended Data Fig. 1b). On the basis of these results and the cytoplasmic localization of SETD3 (Extended Data Fig. 1c), we conclude that SETD3 is not a histone methyltransferase and that it probably targets a non-histone substrate.

Among active PKMTs, SETD3 is most similar to human SETD6[5]. We generated a putative SETD3 catalytic mutant based on this homology (Extended Data Fig. 1a) and performed in vitro methylation assays with ^{3}H-SAM (*S*-adenosyl methionine) on total cytoplasmic extracts with wild-type or mutant SETD3. An approximately 42-kDa band was more prominent in reactions with wild-type SETD3 relative to the mutant (Fig. 1b). A three-step fractionation protocol was used to partially purify the SETD3-dependent activity for mass spectrometry analysis (Extended Data Fig. 1d–g). The ten most abundant hits in the proteomic dataset with molecular weights close to the candidate substrate (Extended Data Fig. 1h and Supplementary Table 1) were expressed as recombinant proteins and directly tested as SETD3 substrates in vitro (Fig. 1c). Of these proteins and other potential substrates, only β-actin was methylated by SETD3 (Fig. 1c and Extended Data Fig. 1i). SETD6 and 10 additional active PKMTs do not methylate actin (Fig. 1d, e and Extended Data Fig. 1j). In addition, SETD3 does not methylate the SETD6 substrate RelA[6] (Fig. 1d). These data identify SETD3 as an enzyme that methylates actin in vitro.

To identify the specific actin residue(s) that are modified by SETD3, in vitro methylated actin was analysed by tandem mass spectrometry; deuterated SAM was used as the methyl donor to distinguish SETD3-catalysed methylation from all other sources. Unexpectedly, no lysine methylation events on actin were observed (Extended Data Fig. 2). We therefore extended the analysis to search for methylation events at other residues (arginine, glutamine, cysteine and histidine) and unambiguously identified incorporation of a single deuterated methyl moiety at His73 of actin (Extended Data Fig. 3a–c). Histidine methylation is known to exist on a limited number of proteins. The only known histidine methyltransferase is the yeast enzyme Hpm1p, which methylates Rpl3 (not actin) and bears no structural resemblance to SETD3[7,8]. However, methylation of actin at His73 (actin-His73me) is a canonical modification present in mammals but not in yeast[1,7,9]. We identified His73me (or equivalent) on actin purified from 10 different model organisms, ranging from worms to plants to humans, that all have a SETD3 homologue, but not in *Saccharomyces cerevisiae*, which lacks SETD3 (Extended Data Fig. 4). Thus, actin-His73me is an evolutionarily conserved modification that is present in a broad range of multicellular eukaryotic organisms.

Mutation of actin His to Ala at position 73 (H73A) prevents methylation by SETD3 (Fig. 2a). Histidine can potentially be methylated on the nitrogen in position 1 (π, N1) or 3 (τ, N3) of the imidazole ring (Fig. 2b); His(3-me) is the physiological modification that is found on endogenous actin. Methylation assays performed on actin peptides that spanned His73 (residues 66–80 of β-actin) and in which His73 was either unmethylated or methylated at the N1 or N3 position (Extended Data Fig. 3d) showed that SETD3 methylated the unmodified peptide (k_{cat}, 0.4 min^{-1}) and the His73(1-me)-containing peptide (at a much slower rate), but not the His73(3-me)-containing peptide, indicating

[1]Department of Biology, Stanford University, Stanford, CA, USA. [2]Department of Microbiology and Immunology, Stanford University School of Medicine, Stanford, CA, USA. [3]Department of Molecular and Cellular Oncology, The University of Texas MD Anderson Cancer Center, Houston, TX, USA. [4]Department of Biochemistry, Stanford University School of Medicine, Stanford, CA, USA. [5]Department of Comparative Medicine, Stanford University School of Medicine, Stanford, CA, USA. [6]Stanford Healthcare, Palo Alto, CA, USA. [7]Department of Pathology, Stanford University School of Medicine, Stanford, CA, USA. [8]Department of Chemical and Systems Biology, Stanford University School of Medicine, Stanford, CA, USA. [9]These authors contributed equally: Alex W. Wilkinson, Jonathan Diep, Shaobo Dai. [10]These authors jointly supervised this work: Xiaodong Cheng, Jan E. Carette, Or Gozani. *e-mail: xcheng5@mdanderson.org; carette@stanford.edu; ogozani@stanford.edu

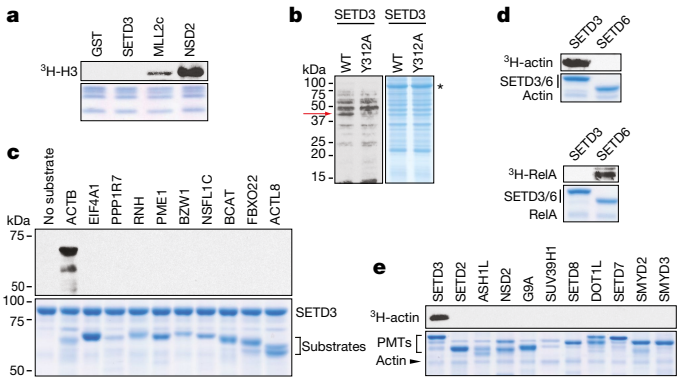

Fig. 1 | SETD3 specifically methylates actin. a, SETD3 does not methylate histones. In vitro methylation reactions on recombinant nucleosomes with recombinant SETD3, minimal MLL2 catalytic complex (MLL2c), the catalytically active NSD2 SET domain, or glutathione-*S*-transferase (GST) as a control. Top, ^{3}H-SAM is the methyl donor and methylation is visualized by autoradiography. Bottom, Coomassie blue stain of nucleosomes used in the reaction. **b**, SETD3 methylates a cytoplasmic protein. In vitro methylation reactions as in **a** with recombinant SETD3 or a putative catalytic mutant (Y312A) using cytoplasmic extracts of HT1080 cells as the substrate. Red arrow, candidate substrate. SETD3 is indicated by the asterisk. **c**, Actin is selectively methylated by SETD3. Methylation assays as in **a** with SETD3 and the indicated recombinant candidate substrates. **d**, Methylation assays with SETD3 and SETD6 on actin and RelA. **e**, Methylation assays with the indicated PKMTs using recombinant β-actin as a substrate. Experiments were independently performed ≥3 times with similar results. For gel source data, see Supplementary Fig. 1.

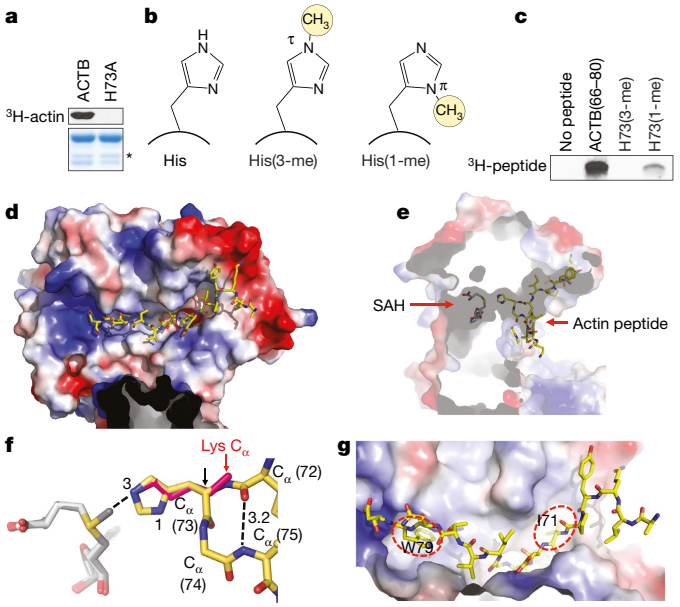

Fig. 2 | SETD3 methylates actin at His73. a, In vitro methylation assay with recombinant wild-type β-actin or H73A mutant. *Non-specific bacterial contaminant. **b**, Histidine methylation: left, histidine; centre, 3-(τ)-methyl histidine; right, 1-(π)-methyl histidine. **c**, SETD3 generates His73(3-me). In vitro methylation reactions with SETD3 on the indicated peptides visualized by autoradiography. **a**, **c**, Experiments were independently performed three times with similar results. **d**–**h**, The molecular basis for SETD3 recognition of actin. **d**, A long surface groove of the SET domain accommodates the actin peptide (stick model). Surface is coloured blue for positive, red for negative and white for neutral charges. **e**, A cut-through view of the SET domain illustrates the cofactor SAH and actin peptide approaching from opposing faces and meeting in the middle of the active-site channel. **f**, A superimposition of SETD6 (showing the SAM and target lysine residue in red) and SETD3 bound to an actin peptide, showing residues immediately before and after His73. Black dashed lines highlight critical inter- and intramolecular interactions. **g**, Close-up view of actin peptide-binding groove with side chains Trp79 and Ile71 inserted into two hydrophobic pockets (circled in red dashed lines). For gel source data, see Supplementary Fig. 1.

that SETD3 catalyses methylation of His73 at the physiologically relevant N3 position (Fig. 2c and Extended Data Fig. 3e–g).

To gain insight into the molecular basis of how SETD3 methylates a histidine substrate, we co-crystallized SETD3 with an actin peptide (residues 66–80) that contains His73 in the presence of *S*-adenosyl-L-homocysteine (SAH). We obtained three highly similar crystal forms, focusing on the highest resolution structure of 1.69 Å (Extended Data Table 1). SETD3 contains two lobes (SET and LSMT-like) forming a V-shaped cleft (Extended Data Fig. 5a). The 15-residue actin peptide occupies an extended surface groove of the SET domain (Fig. 2d), with His73 inserted into the active-site channel positioned to meet SAH from the other end (Fig. 2e). From the viewpoint of the cofactor-binding pocket, the methyl-accepting His73 N3 atom is seen at the bottom of the channel (Extended Data Fig. 5b). Structural superimposition of SETD3 and SETD6[5] reveals that for SETD3, the methyl donor group of SAM points towards and is within the distance of 1.8 Å of the target N3 atom of the imidazole ring (Fig. 2f). An intramolecular hydrogen bond between the main-chain carbonyl oxygen of Glu72 and the main-chain amide nitrogen of Ile75 bends the peptide substrate in a sharp turn at His73. This configuration allows His73 and Gly74 (the smallest residue) to enter deep into the channel and positions the target N3 atom in line with the methyl group and sulfur atom of SAM (Fig. 2f and Extended Data Fig. 5c, d); a linear arrangement comprising the nucleophile, the methyl group and the leaving thioester group in the transition state is required for the S_N2 reaction mechanism used by SAM-dependent methyltransferases[10].

All 15 residues of the actin peptide are bound in the structure (Fig. 2d and Extended Data Fig. 5d), with the SETD3–actin peptide interface consisting of an extensive network of charged/polar and hydrophobic interactions that involve both inter- and intramolecular contacts (Extended Data Fig. 5d–n). For example, Trp79 and Ile71 of actin each fit into hydrophobic pockets on the SETD3 surface (Fig. 2g). This long and ordered peptide–substrate recognition groove for SETD3 is unique compared to other SET domains[11], suggesting that SETD3 would inefficiently accommodate substrates that diverge from actin. Structure-guided point mutations in actin that disrupt the hydrophobic interaction (I71A) or are predicted to interfere with proper positioning of His73 in the catalytic pocket (G74I) impair the ability of SETD3 to methylate actin-His73 and the double mutant (I71A/G74I) abolishes activity (Fig. 3a). Furthermore, although a W79E substitution is tolerated (Extended Data Fig. 5e), SETD3 has no activity on actin I71A/W79E double mutations (Fig. 3a). These data highlight the sensitivity of SETD3 activity on actin to changes in the sequence that includes His73. Indeed, the 15-residue sequence spanning His73 is highly conserved among the six human actin isoforms[9,12] with the only difference being an Ile/Val variation at position 76 that does not affect SETD3 recognition (Extended Data Fig. 5g, o). Accordingly, all actin isoforms are methylated by SETD3 in vitro (Fig. 3b). Finally, the putative SETD3 catalytic mutant is a conserved tyrosine (Tyr312) that participates in forming the active-site pocket (Extended Data Fig. 5d, i, p). This mutant has residual activity; however, mutation of additional conserved residues that are important for SAM binding abolished SETD3 activity (Fig. 3c and Extended Data Fig. 5p).

We next generated a state-specific actin-His73me antibody that selectively recognized His73(3-me) peptides (Extended Data Fig. 6a). The majority of endogenous actin is marked by His73 methylation in HT1080 cancer cells and the depletion of endogenous SETD3 by two independent single-guide RNAs (sgRNAs) results in almost complete loss of this modification, as determined by western blotting and mass spectrometry (Fig. 3d and Extended Data Fig. 6b). We also observed complete loss of actin-His73me in a clonal HeLa cell line in which the SETD3 alleles were disrupted (Fig. 3e and Extended Data Fig. 6c). Furthermore, complementation of *SETD3*-depleted HT1080

cells with CRISPR-resistant wild-type, but not with catalytically dead SETD3(NHY), reconstituted actin methylation at His73 (Fig. 3f and Extended Data Fig. 6d). To assess the physiological role of SETD3 in regulating actin His73 methylation, we obtained *Setd3*$^{+/-}$ mice from the Canadian Mouse Mutant Repository[13] and generated *Setd3* null homozygote mice (*Setd3*$^{-/-}$) that are viable. Analysis of actin purified from nine different tissue types isolated from *Setd3*$^{+/+}$ and *Setd3*$^{-/-}$ mice showed that in tissues that expressed SETD3, the majority of actin is methylated; however, this modification is not detected in any tissue obtained from *SETD3*-deficient mice (Fig. 3g and Extended Data Fig. 7a–d). Finally, quantitative profiling of serum amino acids identified depletion of 3-methyl histidine as the only abnormality in *Setd3*$^{-/-}$ mice (Extended Data Fig. 7e). Collectively, these results identify SETD3 as the physiological actin-His73 methyltransferase.

Actin is one of the more abundant proteins in the human proteome and His73me is a high stoichiometry event. Our data argue that SETD3 is the principal enzyme tasked with generating actin-His73me; however, it remained unclear whether actin-His73 was the only SETD3 substrate or one of many substrates. There are few known histidine-methylated proteins in addition to actin—one is myosin, which SETD3 does not methylate (Fig. 3h). In addition, SETD3 has no activity on histones and several other proteins (Fig. 1c, d and Extended Data Fig. 1i). To investigate the catalytic specificity of SETD3 in a physiological and unbiased setting, we used quantitative proteomics to compare the methylome of HeLa cells with and without SETD3 (Fig. 3e). Of the more than 900 methylation events detected in the analysis, including around 180 histidine methylated peptides (Supplementary Table 2), actin-His73me was the only modification that was quantitatively altered upon SETD3 depletion (Fig. 3i). Together, these results indicate that the principal physiological enzymatic function of SETD3 is actin-His73 methylation.

On the basis of studies that use actin mutants, His73 and its methylation are suggested to influence actin polymerization dynamics, in part owing to its proximity to the ATP-binding site[9,12,14]. However, a direct side-by-side comparison of the properties of actin with and without methylation has, to our knowledge, not previously been possible. We purified actin with and without His73me (Extended Data Fig. 8a, b) from HeLa cells (Fig. 3e) and found that methylation promoted actin polymerization kinetics in vitro but did not affect depolymerization (Fig. 4a and Extended Data Fig. 8c). Moreover, the rate of ATP nucleotide exchange was faster using the unmethylated species (Fig. 4b). We note that actin-His73me exhibited a subtle increase in polymerization when extending off of phalloidin–actin seeds, and made little difference to the polymerization rates in response to porcine Arp2/3 complex stimulation (Extended Data Fig. 8d, e). To explore the role of His73 methylation during actin polymerization in cells, mouse embryonic fibroblasts were isolated from *Setd3*$^{+/-}$ mice that were positive for actin-His73me and *Setd3*$^{-/-}$ mice that lacked methylation (Fig. 4c). Cells that contained actin-His73me were modestly more efficient at migration than cells that were deficient in methylated actin (Fig. 4d and Extended Data Fig. 8f). Together, these data are consistent with a model in which SETD3 methylation of actin positively regulates actin polymerization in cells.

Although *Setd3*$^{-/-}$ mouse embryonic fibroblasts show a defect in cell migration, *Setd3*$^{-/-}$ mice are viable. Therefore, actin-His73me must have a specialized physiological role in vivo that is not essential for basal actin functions. The characterization of *Setd3*-knockout mice by the International Mouse Phenotypic Consortium scored several phenotypes, including moderate skeletal muscle myopathy, abnormal cardiac electrocardiogram and mildly decreased lean mass[13]. We did not observe gross histopathological changes in muscle tissue isolated from young adult *Setd3*$^{-/-}$ mice (Extended Data Fig. 9a, b). Although we did not perform a comprehensive phenotypic analysis, we observed that the litter sizes of female *Setd3*$^{-/-}$ mice, regardless of the genotype of the sire, were significantly smaller than litters from *Setd3*$^{+/+}$ and *Setd3*$^{+/-}$ females (Extended Data Fig. 9c). To explore this observation further, we analysed parturition in *Setd3*$^{-/-}$ or littermate control females that were all mated with wild-type males. Normal parturition was defined as

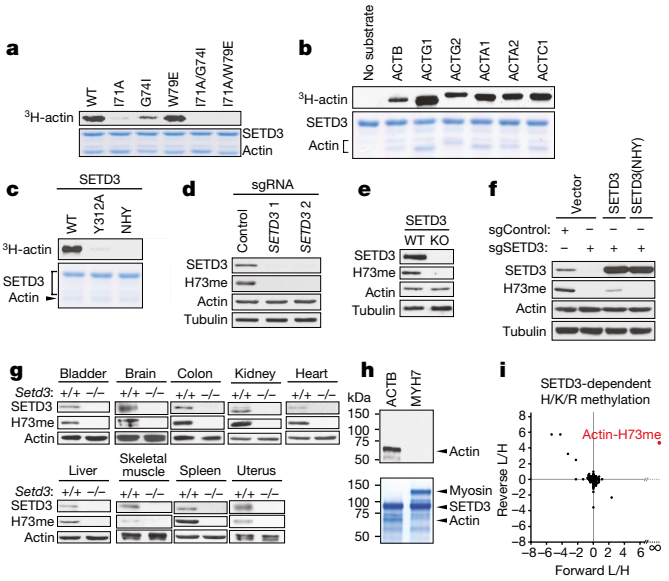

Fig. 3 | SETD3 is the principal enzyme that generates actin-His73me in cells and in vivo. a, In vitro methylation assay with SETD3 on indicated structure-guided actin mutants. **b**, SETD3 methylation reactions on all human actin isoforms. **c**, Analysis of methylation activity of SETD3 mutants: Y312A, catalytic tyrosine; NHY, SAM-binding amino acids (N277A and H278A) and Y312A. **d**, **e**, SETD3 is necessary for His73 methylation in cells. **d**, Western blots, using the indicated antibodies, of HT1080 whole-cell extracts that expressed CRISPR–Cas9 and two independent sgRNAs targeting *SETD3* or a control sgRNA. Actin levels do not change and tubulin is shown as a loading control. **e**, Western blots analysis of whole-cell extracts made from HeLa cells or a clonal *SETD3* knockout. **f**, Western blots of SETD3-deficient HT1080 cells as in **e** complemented with CRISPR-resistant wild-type SETD3 (SETD3(WT)), SETD3(NHY) or control plasmids. **g**, SETD3 mediates actin His73 methylation in vivo. Whole-tissue extracts were made from the indicated tissues from *Setd3*$^{+/+}$ and *Setd3*$^{-/-}$ mice and analysed by western blot. **h**, In vitro reactions with SETD3 and SETD6 on purified β-cardiac myosin sS1 (MYH7) and β-actin as a positive control. **i**, Methylation of actin-His73 is the only change out of more than 900 lysine, arginine and histidine methylation events detected upon *SETD3* depletion in cells. SILAC (stable isotope labelling of amino acids in cell culture)-based quantitative proteomic analysis of methylated peptides in cells with and without SETD3 using HeLa cells from **e**. SILAC ratios from two independent experiments are plotted in the forward direction (*x* axis, $\log_2$-transformed) and the label-swapped reverse direction (*y* axis, $-\log_2$-transformed). Forward: wild-type *SETD3*, light; *SETD3* knockout, heavy. Reverse: wild-type *SETD3*, heavy; *SETD3* knockout, light. SETD3-dependent methylation events are found in the top-right quadrant. For actin-His73me, no heavy peptide was found in the forward direction because of the complete loss of SETD3, so the ratio divisible by zero was plotted as infinite. An actin-His73me ratio is calculated in the reverse direction because of incomplete heavy amino acid labelling cross-contamination. Experiments were independently performed three times with similar results. For gel source data, see Supplementary Fig. 1.

birth at 19 days post-coitum (d.p.c.) and dystocia (delayed parturition) was defined as either no births (≥20 d.p.c.) or incomplete delivery with fetuses remaining in utero (≥20 d.p.c.). Dystocia is normally a rare phenotype; however, it was observed in 8 out of 9 *Setd3*$^{-/-}$ mice, whereas normal parturition was observed for all of the control mice (Fig. 5a). As expected, in control mice, no fetuses were detected in utero at 20 d.p.c. (Fig. 5b). By contrast, *Setd3*$^{-/-}$ females typically had fetuses remaining in utero at ≥20 d.p.c. (Fig. 5b, c).

The dystocia observed in the *Setd3*$^{-/-}$ females is independent of the genotype of the fetus as (1) wild-type males were used as sires; (2) pups successfully born to *Setd3*$^{-/-}$ mice were viable; and (3) *Setd3*$^{+/-}$ females had normal parturition. Thus, the cause of dystocia is of maternal origin. Secondary maternal dystocia is unlikely as there were no obvious and consistent anatomical pelvic abnormalities present in *Setd3*$^{-/-}$ females

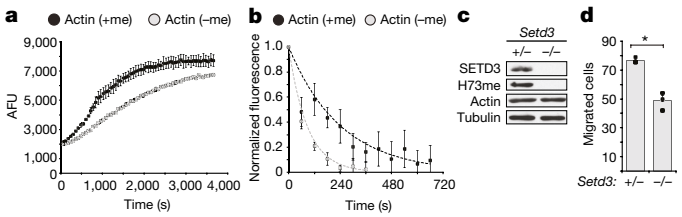

Fig. 4 | His73 methylation regulates actin behaviour. a, **b**, Methylation increases actin polymerization. **a**, Pyrene-labelled skeletal muscle actin was added to the indicated actin in a 1:10 ratio (pyrene:HeLa actin) and polymerization was monitored by arbitrary fluorescence units (AFU) with 5 μM actin. HeLa actin with His73 methylation (+me, black circles); without His73 methylation (−me, grey circles). **b**, ATP exchange rates decrease owing to His73 methylation. Actin saturated with ε-ATP was monitored for exchange with normal ATP by loss of fluorescence over time. Exponential curves (dashed lines) were drawn to the data by least-squares fitting. **c**, **d**, SETD3 promotes cell migration. **c**, Western blot analysis of whole-cell extracts from mouse embryonic fibroblasts isolated from *Setd3*$^{+/-}$ and *Setd3*$^{-/-}$ mice. **d**, Quantification of cell migration assays (see Methods) over a 24-h period. *$P = 0.002$; unpaired two-tailed Student's *t*-test. Data are mean ± s.e.m. of three independent biological replicates. All experiments were independently repeated three times with similar results. For gel source data, see Supplementary Fig. 1.

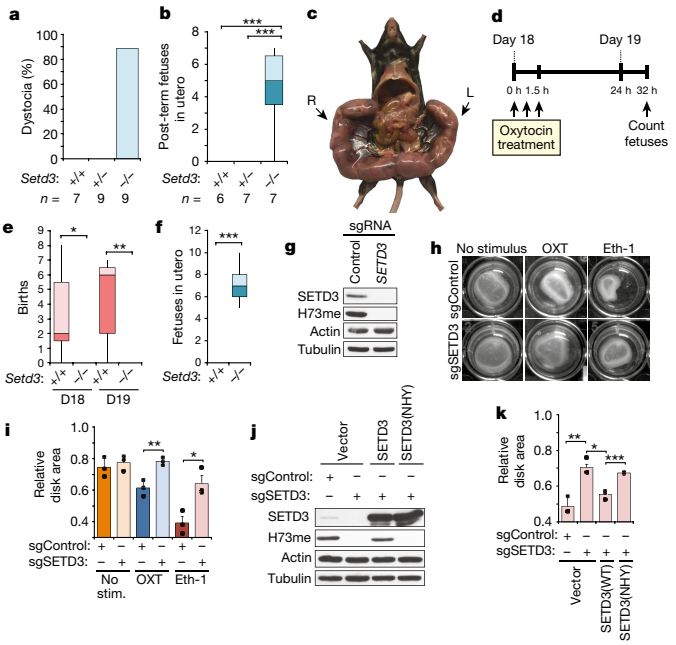

Fig. 5 | SETD3 regulates signal-induced smooth muscle contraction. a–**f**, Primary dystocia in *SETD3*-deficient female mice. **a**, Percentage of pregnant females with dystocia. Genotypes and *n* as noted. **b**, Fetuses that remained in utero were quantified at 20 d.p.c. or 24 h after giving birth for the indicated genotypes. ***$P < 0.0001$; one-way ANOVA with Tukey's multiple comparison test. **c**, Example of a *Setd3*$^{-/-}$ female at 20 d.p.c. from **b** that had not given birth to live pups. Arrows, uteri containing fetuses (right (R), 4 fetuses; left (L), 3 fetuses). **d**–**f**, Labour induction at 18 d.p.c. does not rescue dystocia of *Setd3*$^{-/-}$ pregnant mice. **d**, Schematic of oxytocin treatment protocol. **e**, Quantification of births on days 18 and 19 after oxytocin treatment for *Setd3*$^{+/+}$ ($n = 7$) and *Setd3*$^{-/-}$ ($n = 5$) mice. *$P = 0.042$; **$P = 0.012$. **f**, Quantification of fetuses in utero of mice from **e** (*Setd3*$^{+/+}$, $n = 4$; *Setd3*$^{-/-}$, $n = 5$). ***$P \leq 0.001$. **e**, **f**, *P* values were calculated using unpaired two-tailed Student's *t* tests. **a**, **b**, **e**, **f**, Box and whisker parameters: centre line, median; box limits, upper and lower quartiles; whiskers, maximum and minimum. **g**–**k**, Stimulus-induced contraction requires SETD3 and actin-His73me. **g**, Western blot analysis of primary uterine smooth muscle cells expressing CRISPR–Cas9 and control or *SETD3*-specific sgRNAs. **h**, Representative images of a collagen contraction assay with cells from **g** with or without oxytocin (OXT, 10 μM) or endothelin-1 (Eth-1, 1 μM) after 24 h. **i**, Quantification of **h**. Collagen disk area is measured for indicated conditions and normalized to the area without cells. *$P = 0.019$; **$P = 0.007$. **j**, Western blot analysis of cells from **g** expressing SETD3(WT), catalytically dead SETD3(NHY) or a control vector. **k**, Quantification of contraction assays with reconstituted primary uterine cell lines as described in **i**. *$P = 0.009$; **$P = 0.006$; ***$P = 0.001$. **g**–**k**, Data are mean ± s.e.m. of experiments performed in biological triplicate. *P* values from unpaired two-tailed Student's *t*-tests. All experiments were independently performed three times with similar results. For gel source data, see Supplementary Fig. 1.

and an anatomical defect would not explain the presence of intact fetuses in utero. Thus, the dystocia is primary, either due to abnormal myometrial contractions or a defect in hormone signalling. To distinguish between these possibilities, early labour was induced in wild-type and *Setd3*$^{-/-}$ females using oxytocin administration at 18 d.p.c. (see schematic in Fig. 5d). Wild-type mice went into early labour and all pups were born within 24 h of treatment, whereas the dystocia of *Setd3*$^{-/-}$ mice was refractory to oxytocin (Fig. 5e, f). Similar results were observed with prostaglandin treatment as an independent ecbolic agent[15] (Extended Data Fig. 9d, e). These data identify a specific requirement for SETD3 in the contraction mechanism of the uterus during labour, a mechanism that fundamentally relies on proper actin behaviour[16].

As multiple, unique point mutations in actin are implicated in the aetiology of several human smooth muscle myopathies[17,18], we propose that there is a link between actin-His73me and uterine cell contraction in the primary dystocia of *Setd3*$^{-/-}$ females. To test this idea, we depleted SETD3 and actin-His73me from primary human myometrial cells (Fig. 5g) and measured cellular contraction under normal conditions and in response to two stimulants of uterine smooth muscle contractions. Although depletion of SETD3 had only a small effect on intrinsic contractions, the absence of SETD3 significantly impeded signal-induced contractions by oxytocin and endothelin-1 (Fig. 5h, i). Finally, the loss of endothelin-1-induced cellular contractions upon SETD3 knockdown was rescued in the primary human myometrial cells by complementation with CRISPR-resistant wild-type SETD3, but not by the catalytically inactive SETD3(NHY) (Fig. 5j, k and Extended Data Fig. 9f). These data suggest a specific role for actin-His73me in signal-induced contraction of smooth muscle.

Here we identify SETD3 as a metazoan protein histidine methyltransferase and the enzyme that is responsible for generating actin-His73me. SETD3 represents a SET domain family member that methylates a residue other than lysine, broadening the current framework of possible chemistries catalysed by SET domains. Our analysis reveals that histidine methylation—previously detected on only a handful of proteins—is surprisingly common, observed with a frequency that is similar to that of protein lysine di- and trimethylation[19]. Actin mutations are implicated in smooth muscle myopathies[17,18], including in the case of a pregnant patient who suffered from uterine muscle atony[20]. We propose that SETD3 deficiency and loss of His73me presents, similar to intrinsic actin mutations, by altering actin responsiveness to polymerization cues, which leads to defects in smooth muscle contraction. The effect of His73me on the interactions between actin and myosin is marginal (Extended Data Fig. 9g, h), suggesting that the regulation of smooth muscle contractions is mediated by a different mechanism. Specifically, in addition to the canonical actin–myosin pathway, there is a distinct role for dynamic actin polymerization in mediating mechanical force generation of smooth muscle[21]. In summary, our work identifies a functional role for mammalian histidine methylation in regulating actin and smooth muscle contraction and suggests a broad role for this modification in the regulation of mammalian proteomes.

Online content

Any Methods, including any statements of data availability and Nature Research reporting summaries, along with any additional references and Source Data files, are available in the online version of the paper at https://doi.org/10.1038/s41586-018-0821-8.

Received: 24 March 2018; Accepted: 30 November 2018;
Published online 10 December 2018.

1. Johnson, P., Harris, C. I. & Perry, S. V. 3-methylhistidine in actin and other muscle proteins. *Biochem. J.* **103**, 79P (1967).
2. Seaborne, R. A. et al. Human skeletal muscle possesses an epigenetic memory of hypertrophy. *Sci. Rep.* **8**, 1898 (2018).
3. Carlson, S. M. & Gozani, O. Nonhistone lysine methylation in the regulation of cancer pathways. *Cold Spring Harb. Perspect. Med.* **6**, a026435 (2016).
4. Eom, G. H. et al. Histone methyltransferase SETD3 regulates muscle differentiation. *J. Biol. Chem.* **286**, 34733–34742 (2011).
5. Chang, Y. et al. Structural basis of SETD6-mediated regulation of the NF-kB network via methyl-lysine signaling. *Nucleic Acids Res.* **39**, 6380–6389 (2011).
6. Levy, D. et al. Lysine methylation of the NF-κB subunit RelA by SETD6 couples activity of the histone methyltransferase GLP at chromatin to tonic repression of NF-κB signaling. *Nat. Immunol.* **12**, 29–36 (2011).
7. Clarke, S. G. Protein methylation at the surface and buried deep: thinking outside the histone box. *Trends Biochem. Sci.* **38**, 243–252 (2013).
8. Webb, K. J. et al. A novel 3-methylhistidine modification of yeast ribosomal protein Rpl3 is dependent upon the YIL110W methyltransferase. *J. Biol. Chem.* **285**, 37598–37606 (2010).
9. Kalhor, H. R. et al. A highly conserved 3-methylhistidine modification is absent in yeast actin. *Arch. Biochem. Biophys.* **370**, 105–111 (1999).
10. Schubert, H. L., Blumenthal, R. M. & Cheng, X. Many paths to methyltransfer: a chronicle of convergence. *Trends Biochem. Sci.* **28**, 329–335 (2003).
11. Del Rizzo, P. A. & Trievel, R. C. Substrate and product specificities of SET domain methyltransferases. *Epigenetics* **6**, 1059–1067 (2011).
12. Yao, X., Grade, S., Wriggers, W. & Rubenstein, P. A. His^{73}, often methylated, is an important structural determinant for actin. A mutagenic analysis of His^{73} of yeast actin. *J. Biol. Chem.* **274**, 37443–37449 (1999).
13. Dickinson, M. E. et al. High-throughput discovery of novel developmental phenotypes. *Nature* **537**, 508–514 (2016).
14. Nyman, T. et al. The role of MeH73 in actin polymerization and ATP hydrolysis. *J. Mol. Biol.* **317**, 577–589 (2002).
15. Narver, H. L. Oxytocin in the treatment of dystocia in mice. *J. Am. Assoc. Lab. Anim. Sci.* **51**, 10–17 (2012).
16. Smith, R., Imtiaz, M., Banney, D., Paul, J. W. & Young, R. C. Why the heart is like an orchestra and the uterus is like a soccer crowd. *Am. J. Obstet. Gynecol.* **213**, 181–185 (2015).
17. Guo, D. C. et al. Mutations in smooth muscle alpha-actin (*ACTA2*) cause coronary artery disease, stroke, and Moyamoya disease, along with thoracic aortic disease. *Am. J. Hum. Genet.* **84**, 617–627 (2009).
18. Milewicz, D. M. et al. De novo *ACTA2* mutation causes a novel syndrome of multisystemic smooth muscle dysfunction. *Am. J. Med. Genet. A* **152A**, 2437–2443 (2010).
19. Cao, X. J., Arnaudo, A. M. & Garcia, B. A. Large-scale global identification of protein lysine methylation in vivo. *Epigenetics* **8**, 477–485 (2013).
20. Cooper, K. & Brown, S. *ACTA2* mutation and postpartum hemorrhage: a case report. *BMC Med. Genet.* **18**, 143 (2017).
21. Gunst, S. J. & Zhang, W. Actin cytoskeletal dynamics in smooth muscle: a new paradigm for the regulation of smooth muscle contraction. *Am. J. Physiol. Cell Physiol.* **295**, C576–C587 (2008).

Acknowledgements We thank J. Drozak and colleagues for sharing their independent identification of SETD3 as the actin-His73 methyltransferase[22] and members of the Gozani laboratory for critical reading of the manuscript. This work was supported in part by grants from the NIH to O.G. (R01 GM079641), J.E.C. (DP2 AI104557 and U19 AI109662), X.C. (R01 GM114306), J.A.S. (GM33289), and a CPRIT grant to X.C. (RR160029). J.E.E. received support from Stanford ChEM-H. J.E.C. is supported by an AAF Scholar Award.

Reviewer information *Nature* thanks S. Richard and the other anonymous reviewer(s) for their contribution to the peer review of this work.

Author contributions A.W.W. performed biochemical and molecular experiments, and was responsible for experimental design and execution, data analysis and manuscript preparation. A.W.W. performed and analysed mass spectrometry experiments with help from S.L., T.-M.L. and J.E.E. C.M.N. and J.D. performed mouse experiments with help from Y.S.O. K.M.C. and J.G.V.-M. performed histopathology. J.M. and T.C. analysed plasma amino acids. S.D., J.R.H., X.Z. and X.C. performed kinetic experiments and determined X-ray structures. D.S., D.V.T. and C.L. provided myosin and analysed actin–myosin interactions, supervised by K.M.R. and J.A.S. O.G., J.E.C. and X.C. supervised the research, interpreted data and prepared the manuscript.

Competing interests O.G. is a co-founder of EpiCypher Inc. and Athelas Therapeutics Inc.

Additional information

Extended data is available for this paper at https://doi.org/10.1038/s41586-018-0821-8.
Supplementary information is available for this paper at https://doi.org/10.1038/s41586-018-0821-8.
Reprints and permissions information is available at http://www.nature.com/reprints.
Correspondence and requests for materials should be addressed to X.C., J.E.C. or O.G.
Publisher's note: Springer Nature remains neutral with regard to jurisdictional claims in published maps and institutional affiliations.

METHODS

Reagents. Biotinylated peptides were synthesized at the UNC High-Throughput Peptide Synthesis and Array Facility[23]. Fmoc-L-histidine amino acids with either 1-me or 3-me modifications (Sigma-Aldrich) were used in the synthesis of these peptides and synthesized peptides were purified by high-performance liquid chromatography (>92% purity). The following antibodies were used in this study: SETD3 (Abcam), pan-actin (Cytoskeleton), β-tubulin (Millipore), H3K4me2 (Cell Signaling), H3K36me2 (Cell Signaling), His73(3-me) (see below), GFP (Invitrogen), Alexa488 anti-rabbit antibody (Life Technologies), anti-rabbit and anti-mouse peroxidase-conjugated antibodies (Jackson Immunoresearch). Western blots were visualized by chemiluminescence (GE Healthcare).

Anti-His73(3-me)-specific antibody generation. A peptide that corresponds to amino acids 68–78 of β-actin (KYPIEHGIVTN) with His(3-me) at position 73 was synthesized and purified by high-performance liquid chromatography (99% purity). This peptide was conjugated to KLH and used as antigen to immunize rabbits. Rabbit protocols, peptide conjugation, immunization and antiserum production were performed by Pocono Rabbit Farm & Laboratory. Antiserum was negatively selected against an unmodified actin peptide (amino acids 66–80). Final purification with was performed with an immobilized antigenic peptide to select for His73(3-me)-specific antibodies.

Recombinant protein expression for in vitro reactions. SETD3 (Uniprot ID: Q86TU7) and actin were cloned into pGEX-6P-1. The MLL2 catalytic complex contained the GST-tagged catalytic SET domain of MLL2, as well as full-length, 6×His-tagged ASH2L, WDR5, DPY30 and RBBP5 proteins that were all individually expressed in bacteria and assembled in stoichiometric proportions to result in a catalytic complex[24]. Lysine methyltransferases that were used as controls were reacted with previously reported substrates[25–36]. Candidate substrate cDNAs were subcloned from the human ORFeome (Open Biosystems) using an LR recombination reaction (Life Technologies) into pDEST15. Mutations of all proteins were generated using Phusion site-directed mutagenesis (Thermo Scientific) according to the manufacturer's recommendations. All proteins were expressed as N-terminal GST fusions (except for non-catalytic MLL complex components) in BL21 or BL21(DE3) codon-plus bacteria. Expression was performed overnight at 16 °C in the presence of 0.1 mM IPTG. Recombinant GST fusions were purified with Glutathione Sepharose 4B (GE Healthcare) and eluted in 100 mM Tris pH 8.0, 10 mg ml^{-1} reduced glutathione (Sigma-Aldrich). Any cleavage of GST tags was performed with PreScission Protease (GE Healthcare) overnight at 4 °C. Recombinant 6×His-tagged proteins were purified with Ni-NTA agarose (Life Technologies) and eluted in 100 mM Tris pH 8.0 and 250 mM imidazole. Kinetics experiments and crystallography used additional purification steps as described below.

Purification of SETD3 for crystallography. SETD3 was expressed as a GST-fusion protein as described above. Cleared bacterial lysates that contained the soluble GST-fused SETD3 were first loaded on a self-packed glutathione-sepharose column and eluted with buffer containing 100 mM Tris (pH 8.0), 150 mM NaCl, 5% glycerol, 0.5 mM TCEP and 20 mM reduced glutathione. The GST tag was removed by approximately 100 μg PreScission Protease (purified in-house) at 4 °C overnight. The cleaved protein solution was diluted to around 50 mM NaCl and further purified by HiTrap Q-HP (GE Healthcare) with a linear gradient from 50 mM to 500 mM NaCl; SETD3 eluted together with cleaved GST around 200–300 mM NaCl. To remove GST, fractions were loaded onto a fresh glutathione-sepharose column and the flow through was collected and concentrated to around 2 ml. SETD3 was then further purified by size-exclusion chromatography (Superdex 200, GE Healthcare) in 20 mM Tris (pH 8.0), 200 mM NaCl, 5% glycerol, 0.5 mM TCEP. All purification steps were performed at 4 °C. The chromatography experiments were conducted in a BIO-RAD NGCTM system.

Cellular fractionation. Cytoplasmic cellular extracts were prepared using established protocols[37]. In brief, cells were disrupted by hypotonic lysis (25 mM KCl, 1.5 mM $MgCl_2$, 10 mM HEPES–KOH pH 7.9 and protease inhibitors) and dounce homogenization. Size-exclusion chromatography (Superose 6) was performed in hypotonic lysis buffer. Ion-exchange chromatography (Sepharose Q HP) columns were equilibrated in hypotonic lysis buffer and proteins were eluted on a linear gradient from 25 to 600 mM KCl. Fractions were concentrated with centrifugal filter units (Amicon, 3,000 Da molecular weight cut-off) before being used as substrate in in vitro reactions with radiolabelled SAM. Chromatography for substrate enrichment was performed with an AKTA FPLC (GE Healthcare).

In vitro methylation reactions. In vitro methyltransferase reactions were performed with 5 μg methyltransferase, 1 μg substrate, and 2 μCi ^{3}H-*S*-adenosylmethionine (American Radiolabelled Chemicals) in a buffer that contained 50 mM Tris pH 8.0, 20 mM KCl and 5 mM $MgCl_2$ and were incubated at 30 °C overnight. Reactions were resolved by SDS–PAGE and ^{3}H-methylation was visualized by autoradiography and gels were stained with Coomassie blue as a loading control. Reactions with deuterated SAM (CDN Isotopes) or normal SAM (Sigma-Aldrich) were performed with SAM at a final concentration of 80 μM.

Steady-state kinetic measurements. Human β-actin peptide (residues 66–80; TLKYPIEHGIVTNWD) was used as a substrate for SETD3. The reaction mixture contained 20 mM Tris (pH 8.0), 50 mM NaCl, 0.1 mg ml^{-1} BSA, 1 mM DTT and 0.18 μM SETD3. To determine the Michaelis constant (K_m) value of the peptide, the concentration of SAM was kept constant at 40 μM, whereas for the determination of the K_m of SAM, the peptide concentration was kept constant at 50 μM. Reactions were carried out at room temperature for 20 min with a total volume of 20 μl, and terminated by the addition of trifluoroacetic acid to 0.1% (v/v). The activity of SETD3 was measured using a bioluminescence assay (MTase-Glo, Promega) in which the reaction by-product SAH is converted into ATP in a two-step reaction and ATP can be detected through a luciferase reaction[38]. In general, 5 μl of reaction mixture was transferred to a low-volume 384-well plate and the luminescence assay was performed according to the manufacturer's protocol. A Synergy 4 Multi-Mode Microplate Reader (BioTek) was used to measure luminescence signals.

Time course of methylation for three β-actin peptides. Typically, a reaction mixture contained 20 mM Tris (pH 8.0), 50 mM NaCl, 0.1 mg ml^{-1} BSA, 1 mM DTT, 40 μM SAM and 50 μM peptide. In addition to the unmodified peptide, 1-methyl-His and 3-methyl-His peptides were used in the activity assay. For the unmodified peptide, 0.18 μM SETD3 was used, whereas for modified peptides, 80-fold higher amounts of SETD3 (14.4 μM) were used owing to very low activity on these peptides. For each time point, 10 μl of reaction mixture was taken and trifluoroacetic acid was added to 0.1% to stop the reaction. The luminescence assay was performed as described above.

Mass spectrometry. Liquid chromatography–tandem mass spectrometry (LC–MS/MS) was performed using an Orbitrap Elite or Fusion (Thermo Scientific) and data were analysed manually or using MaxQuant software[39]. Searches to identify peptides using MaxQuant were performed with parameters to identify methionine oxidation, *N*-acetylation, monomethyl lysine, dimethyl lysine, trimethyl lysine, methyl histidine, monomethyl arginine, dimethyl arginine, methyl glutamine and methyl cysteine. In vitro reactions were directly resolved by SDS–PAGE before mass spectrometry analysis was performed as described above and digested with trypsin, chymotrypsin or Glu-C (Promega). Quantitative proteomic analysis was performed with SILAC, light isotopic labels (K0R0) and heavy isotopic labels (K8R10). In the SETD3-dependent methylomics experiments, no peptides with a SILAC ratio greater than 1.5 were deemed to be SETD3-dependent methyl events. No peptides (other than actin) with at least a 1.5-fold ratio in the reverse direction and NaN ratio in the forward direction were identified at all in the forward direction. Actin His73 methylation was detected with light (wild-type cells, K0R0) labelling in the forward direction and not with heavy labelling (SETD3 knockout cells, K8R10). We thus concluded that the lack of a calculable ratio (light/heavy) in the forward direction is due to the clonal nature of the cell lines being used. We therefore plotted the forward ratio as infinite (Fig. 3i).

Targeted quantification of actin methylation was performed by manual identification of methylated and unmethylated peptides followed by integration of the area under the curve for chromatographic peaks associated with the corresponding *m*/*z*. The percentage of methylated peptides was determined as a fraction of the sum of the total area for methylated and unmethylated species. Actin was isolated from cellular or tissue sources using DNase I affinity chromatography[40]. DNase I was immobilized on NHS-activated Sepharose FF (GE Healthcare) overnight in 100 mM HEPES pH 7.5, 150 mM NaCl and 80 mM $CaCl_2$. Cells and tissues were homogenized using a buffer that contained 1 M Tris pH 8.0, 600 mM KCl, 0.5 mM $MgCl_2$, 4% NP-40, 1% Tween-20, 1 mM DTT, 1 mM ATP and protease inhibitors[41] (Roche). Cleared lysates were incubated with immobilized DNase I resin overnight, washed, boiled in SDS sample buffer and purified actin was resolved by SDS–PAGE. Gels were silver-stained (Thermo Scientific) after which actin bands were excised and processed for mass spectrometry by in-gel digestion with sequencing-grade trypsin. The following sources were used for the analysis of actin methylation across evolution: *S. cerevisiae*, mid-log BY4741; *Arabidopsis thaliana*, leaf tissue; *Nicotiana benthamiana*, leaf tissue; *Caenorhabditis elegans*, mixed population; *Drosophila melanogaster*, larvae; *Spodoptera frugiperda*, Sf9 cells; *Danio rerio*, five days post-fertilization embryos; *Xenopus laevis*, egg extract; *Gallus gallus*, skeletal muscle; *Mus musculus*, brain tissue as well as uterine and skeletal muscle tissues; *Homo sapiens*, cell lines.

Crystallography. Crystallization of the SETD3–SAH–actin peptide (residues 66–80; Genscript) complex was carried out using the hanging-drop vapour-diffusion method at 20 °C after mixing SETD3 (approximately 15 mg ml^{-1}) with SAH and peptide at a molar ratio of 1:4:5. This mixture was then mixed with an equal amount of crystallization solution. Three different crystal forms were obtained. Crystals with space group $P2_1$ were obtained with 0.2 M ammonium acetate, 0.1 M sodium citrate tribasic dihydrate pH 5.6 and 30% (w/v) polyethylene glycol 4000. Crystals with space group $P2_12_12_1$ were obtained with two similar conditions, either 0.2 M ammonium sulfate or 0.2 M sodium chloride, 0.1 M Bis-Tris pH 5.5, 25% (w/v) polyethylene glycol 3350 and 0.1 M Bis-Tris pH 5.5, 25% (w/v) polyethylene glycol 3350. The first form, like the $P2_1$ crystal, contained

two SETD3–SAH–peptide complexes per asymmetric unit, whereas the second contained only one complex.

For X-ray diffraction data collection, single crystals were flash-frozen in liquid nitrogen by equilibrating in a cryoprotectant buffer that contained crystallization solution with 25% (v/v) ethylene glycol. All datasets were collected at the SER-CAT beamline 22ID of Advanced Photon Source at Argonne National Laboratory. Crystallographic datasets were processed with HKL2000[42]. Molecular replacement was performed with the PHENIX PHASER module[43] using the structure of human SETD3 in complex with SAM (Protein Data Bank (PDB) 3SMT) as a search model. PHENIX REFINE[44] was used for refinement with 5% randomly chosen reflections for validation by the R_{free} value. COOT[45] was used for peptide building and model corrections between refinement rounds. Structure quality was analysed during PHENIX refinements and later validated by the PDB validation server. Molecular graphics were generated using PyMOL (Schrödinger).

We note that the high-resolution data at 1.69 Å (PDB 6MBK) were the result of merging two datasets that were collected from two different parts of the same crystal. This crystal did diffract X-rays to a higher resolution but was susceptible to radiation damage, especially in the higher resolution range. The merge resulted in 98.4% completeness in the highest resolution shell of 1.75–1.69 Å. The slightly higher R_{work} and R_{free} values of the structure (PDB 6MBK) might be an indication of radiation damage that could not be modelled and further refinement would not lower these R values substantially and the structure and map compared well with the quality of the other two crystal forms.

Actin purification for biochemical assays. Actin was purified from wild-type HeLa cells or a clonally derived HeLa cell line in which SETD3 was knocked out. Purification was adapted from established protocols[46]. In brief, HeLa cells were resuspended in lysis buffer (10 mM Tris-HCl pH 8.0, 11.6% (w/v) sucrose, 1 mM EGTA, 1 mM ATP, 5 mM DTT and protease inhibitor cocktail) and lysed by sonication. Lysates were cleared by ultracentrifugation (100,000*g*, 2 h). Cleared cellular extracts were loaded onto an anion-exchange column (Sepharose Q HP, GE Healthcare) equilibrated with column buffer (10 mM Tris-HCl pH 8.0, 0.2 mM $CaCl_2$, 0.5 mM ATP and 0.5 mM DTT). Actin protein was eluted on a linear gradient of column buffer containing 0 mM KCl to column buffer containing 600 mM KCl. Actin-positive fractions were polymerized with 2 mM $MgCl_2$ and 1 mM ATP at room temperature, and polymerized actin was pelleted at 100,000*g* for 2 h. F-actin was resuspended and depolymerized in 2 mM Tris pH 8.0, 0.2 mM $CaCl_2$, 0.5 mM DTT and 0.2 mM ATP for $\geq$2 days. Residual F-actin was cleared by ultracentrifugation as described above and the protein in the supernatant was used in biochemical assays.

Pyrene-based polymerization assays were performed according to commercially available kit instructions (Cytoskeleton). Purified HeLa actin was combined in a 10:1 ratio with pyrene-labelled actin from rabbit skeletal muscle (Cytoskeleton). Polymerization was induced with 2 mM $MgCl_2$, 50 mM KCl and 1 mM ATP, and monitored by fluorescence in a plate reader (excitation, 355 nm; emission, 410 nm; Biotek Cytation 3, Gen5 v.3.04.17 software). Readings were taken every 60 s with orbital shaking. Depolymerization assays were performed by diluting actin that was polymerized as described above by 250-fold in 10 mM Tris pH 8.0, 0.2 mM $CaCl_2$ and 1 mM ATP. Depolymerization was monitored by fluorescence similar to polymerization. Phalloidin–actin seeds were made by polymerizing monomeric actin into filaments followed by incubation of the resulting F-actin with a stoichiometric excess of phalloidin (Millipore-Sigma). F-actin was pelleted for 1 h at 100,000*g*. F-actin was washed and resuspended in F-buffer (10 mM Tris pH 7.5, 2 mM $MgCl_2$, 50 mM KCl, 1 mM ATP and 1 mM DTT) and then sheared through a 27G needle. Seeds were allowed to recover overnight at room temperature. Polymerization with seeds was performed with 2 μM seed, 1 μM monomeric actin and 0.1 μM pyrene–actin. Polymerization with Arp2/3 complex (Cytoskeleton) and recombinant WASP VCA (the verprolin, cofilin and acidic domains of the Wiskott–Aldrich Syndrome Protein) (Cytoskeleton) were used at concentrations of 5 nM and 100 nM, respectively, with 1 μM actin and 0.1 μM pyrene–actin.

Nucleotide exchange. Nucleotide exchange assays were performed as previously reported[47]. G-actin monomers were transferred into a buffer without ATP (2 mM Tris pH 7.5, 0.2 mM $CaCl_2$, 1 mM DTT) by desalting column (GE Healthcare, PD spin column with G-25). 1,N^6-ethenoadenosine-5′-*O*-triphosphate (ε-ATP, Axxora) was added to G-actin at a final concentration of 0.3 mM and incubated on ice for at least 2 h. Unbound ε-ATP was removed by desalting as described above. ATP exchange of ε-ATP with normal ATP (100 μM) was performed with 2 μM G-actin and monitored by fluorescence (excitation, 340 nm; emission, 410 nm) in triplicate.

Cell culture. HEK293T (ATCC), HT1080 (ATCC) and H1-HeLa (ATCC) cells were cultured in Dulbecco's modified Eagle's Medium (DMEM, Life Technologies) supplemented with 10% fetal bovine serum, 2 mM L-glutamine and penicillin–streptomycin (Life Technologies). Primary uterine smooth muscle cells (ATCC) were cultured in vascular cell basal medium (ATCC) supplemented with the vascular smooth muscle growth kit (ATCC). All above cell lines were authenticated and declared mycoplasma free by ATCC. Transfections were performed with either TransIT-293 or TransIT-LT1 (Mirus) in HEK293T cells or HT1080 cells, respectively. Stable cell lines were generated using lentiviral transductions. HEK293T cells were co-transfected with the lentiviral plasmid, pCMV-Δ8.2 and pCMV-VSVg in a ratio of 9:8:1 by mass. After 48 h of transfection, target cells were transduced with 0.45-μm-filtered viral supernatants supplemented with 8 μg ml^{-1} polybrene. Viral concentration was performed as necessary with Lenti-X lentiviral concentration solution as per the manufacturer's recommendations (Takara). Cells were selected 24 h after medium replacement. To deplete cells of SETD3, CRISPR–Cas9 components were stably expressed in HT1080 cells using lentiCRISPRv2 (Addgene) with the following single guide (sg)RNAs: control sgRNA, 5′-CTTCGAAATGTCCGTTCGGT-3′; *SETD3* sgRNA 1, 5′-TGTTACAGAATGCAGCAGTC-3′; *SETD3* sgRNA 2, 5′-GTATGTGCAGATCCGGACTC-3′. *SETD3* sgRNA 1 was used for reconstitution experiments and generation of the clonal H1-HeLa cell line. Cell selection was performed with 2 μg ml^{-1} puromycin or 100 μg ml^{-1} hygromycin. *SETD3* cDNA cloned into pLenti CMV Hygro DEST (W117-1) (Addgene) was made CRISPR–Cas9-resistant by incorporating a synonymous mutation into the PAM sequence associated with *SETD3* sgRNA 1 from CGG to CTG. Reconstitution experiments were performed by transient transfection in HT1080 cells or stable incorporation by lentivirus in primary uterine smooth muscle cells. SILAC cell culture was performed with DMEM for SILAC (Thermo Scientific), supplemented with 10% dialysed fetal bovine serum, 115 mg proline (Applichem), 50 mg lysine (light, lysine HCl (Applichem); heavy, $^{13}C_6$,$^{15}N_2$-L-lysine HCl (Silantes)) and 50 mg arginine (light, arginine HCl (Applichem); heavy, $^{13}C_6$,$^{15}N_4$-L-arginine HCl (Silantes)). Cells used for SILAC-based proteomics were cultured in SILAC medium for at least one week before analysis.

Immunofluorescence imaging. H1-HeLa cells were seeded overnight onto autoclaved 12-mm circle micro cover glasses (VWR) at 50,000 cells per well in 24-well plates (Greiner Bio-One). Samples were fixed with 4% paraformaldehyde (Sigma-Aldrich) for 30 min at room temperature. Each sample was incubated with anti-GFP antibody (1:300) in immunofluorescence blocking buffer (1× phosphate-buffered saline (PBS) with 3% BSA, 1% saponin and 1% Triton X-100) overnight at 4 °C. Cells were washed thoroughly with 1× PBS and then incubated for 1 h at room temperature with Alexa488 anti-rabbit antibody (1:500) and DAPI (Insitus Biotechnologies, 1:300 dilution) in immunofluorescence blocking buffer. Washed micro cover glasses were then mounted onto microscope slides (Fisher Scientific) using Vectashield with DAPI (Vector Laboratories). Images were taken with a Zeiss LSM 700 confocal microscope and processed with Volocity software.

Generation of the mouse embryonic fibroblast cell line. Embryos were collected 13.5 d.p.c. and internal organs were removed. The remaining tissues of the embryos were minced and treated with trypsin to dissociate cells for 30 min at 37 °C. Trypsinization was quenched with growth medium (DMEM containing 10% fetal bovine serum). Quenched cell suspensions were plated and allowed to grow for four days. At this point, cells were frozen or used in experiments. Genotyping of new cell lines was performed with residual embryonic tissue and confirmed by western blot analysis.

Cell migration assays. Cell migration assays were performed with Radius cell migration kits (Cell Biolabs). Mouse embryonic fibroblasts (1×10^5 cells) were plated in 24-well migration plates and allowed to attach overnight. The Radius gel was removed according to the manufacturer's protocol. After gel removal, imaging was performed over a 24-h period with a Nikon Eclipse Ti inverted fluorescence microscope and NIS Elements (version 4.60) software. During image acquisition, the environmental conditions were kept at 5% CO_2 and 37 °C (Okolab). After the 24-h period, cells were fixed and stained with DAPI according to kit instructions. Cell migration was quantified by re-imaging migration fields and counting DAPI-stained nuclei within the boundary of the circular void left by the gel at 0 h. Migration assays were performed in triplicate.

Cell contraction assays. Cellular contraction assays were performed on a collagen substrate (Cell Biolabs). In brief, 450 μl collagen mixture made with the provided 5× PBS was added to a 24-well plate and allowed to polymerize according to the manufacturer's protocol. Primary uterine smooth muscle cells (5×10^4 cells) were layered on top of a collagen matrix in vascular basal medium without the growth kit. Cells were allowed to attach to the collagen overnight at 37 °C. The next day, the collagen disks were released from the sides of each well. Induction of contraction was performed with 10 μM oxytocin (Tocris) or 1 μM endothelin-1 (Tocris). Contraction was monitored by imaging after 24 h of contraction. Quantification of collagen disk area was performed in ImageJ (NIH). Relative disk area was determined by normalizing to the area of disks that lacked cells. All assays were performed in triplicate.

Ethics statement. Mice were housed in the Stanford mouse facility accredited by the Association for Assessment and Accreditation of Laboratory Animal Care. All experiments were approved by Stanford's Institutional Animal Care and Use Committee.

Maintenance of mouse colonies. Husbandry is performed in accordance with the Guide for the Care and Use of Laboratory Animals, 8th edition (2010) and the 2015 revision of the Public Health Service Policy on Humane Care and Use of Laboratory Animals. Room conditions included a temperature of 23 °C, relative humidity of 30–40% and a 12:12-h light:dark cycle (lights on, 07:00). All mouse colonies are maintained under specific pathogen-free conditions in irradiated disposable individually ventilated cages (Innocage, Innovive) with irradiated, corncob bedding, irradiated food (Teklad 2918 Global 18% Protein Rodent Diet, Envigo) and ultraviolet-light-irradiated, acidified (pH 2.5–3.0), reverse-osmosis-purified bottled water (Aquavive, Innovive). The mouse colonies are monitored for viral, bacterial and parasitic pathogens using dirty-bedding sentinels that were tested quarterly and were found to be free of mouse parvovirus, minute virus of mice, mouse hepatitis virus, mouse rotavirus, Theiler's murine encephalomyelitis virus, murine norovirus, Sendai virus, mouse adenovirus 1 and 2, ectromelia virus, lymphocytic choriomeningitis virus, pneumonia virus of mice, respiratory enterovirus III, fur mites, lice and pinworms. Sample size was maximized as much as possible to gain highest confidence in the results. No randomization was necessary as only single variables changed per experiment. Blinding was not necessary as any phenotypic assessment or other measurements was performed using discrete, quantitative measurements.

Mouse strains. *Setd3*$^{tm1.1(NCOM)Mfgc}$/Tcp C57BL/6N heterozygous mice were obtained from the Canadian Mouse Mutant Repository (CMMR). The strain was made at the Toronto Centre for Phenogenomics as part of the NorCOMM2 project using NorCOMM embryonic stem cells[48]. Progeny were genotyped using either the Setd3-McKerlie PCR assay to identify the 212-bp wild-type band (primers: *Setd3* WT F1 AACCAGCAGTGCACAGAGACAAGCTG; *Setd3* WT R1 AACCCAAACTCTGCCAGCCAAAGCAC) and/or a 566-bp tm1.1 band (primers: *Setd3* tm1 F4 AAACTGGTGCTGCTGATAACCTGGGC; GH717 CACCGACGCCAATCACAAACAC) following instructions provided by the CMMR or the use of a commercial genotyping service (Transnetyx). For timed pregnant matings, C57BL/6N male mice were purchased from Charles River Laboratories. Male mice began breeding at 8 weeks and female mice at 6 weeks. Typically, mice no older than 6 months were used in this study.

Quantification of litter size and length of gestation. Quantification of pregnancies and litters for both trio- or pair-breeding females were tabulated for *Setd3*$^{-/-}$, *Setd3*$^{+/-}$ and *Setd3*$^{+/+}$ females. All litters that were observed (confirmed) were counted, even if pups subsequently died. To determine the number of pups per litter, litters that were lost before the pups could be counted were listed as 0 pups for that litter. The length of gestation for *Setd3*$^{-/-}$, *Setd3*$^{+/-}$ and *Setd3*$^{+/+}$ females was determined by timed pregnant matings. Females were mated to wild-type C57BL/6N males (Charles River Laboratories). Whether the female was a virgin (primigravida) or had a previous pregnancy (multigravida) was recorded. Presence of a vaginal plug was denoted 0 d.p.c. Plugged females were moved to a separate cage and weights taken at intervals to confirm pregnancy. A few days before 19 d.p.c., the female was placed in a separate cage and provided with nesting material (Enviro-dri, Shepherd Speciality Papers) and a paper tube. Cages were checked for births twice daily (morning and afternoon) starting from 18 d.p.c.

Quantifying dystocia and fetuses in utero. The day of parturition for *Setd3*$^{-/-}$ females varied from 19 d.p.c. to ≥20 d.p.c. Normal parturition was defined as birth at 19 d.p.c. and dystocia (delayed parturition) was defined as either no births (≥20 d.p.c.) or incomplete delivery with fetuses remaining in utero (≥20 d.p.c.). To determine whether *Setd3*$^{-/-}$ females that delivered on 19 d.p.c. still exhibited a delayed in parturition, females were euthanized on late 20 d.p.c. if they did not deliver on 19 d.p.c. (*Setd3*$^{-/-}$) or 24 h after giving birth if they delivered on 19 d.p.c. (*Setd3*$^{-/-}$, *Setd3*$^{+/-}$ and *Setd3*$^{+/+}$) and examined for the presence of fetuses in utero. We note that the dystocia occurred in both primigravida and multigravida *Setd3*$^{-/-}$ females and that actin-His73me is not detected in the uterus of late-stage pregnant *Setd3*$^{-/-}$ females (data not shown).

Induction of parturition. Oxytocin (VetOne, MWI Veterinary Supply Co.) was given subcutaneously on 18 d.p.c. to induce preterm labour (dose, 0.4 U in 0.9% saline supplemented with 0.1% calcium gluconate and 0.025% dextrose, given in a total of 3 injections (once every 30 min over a period of 1.5 h) to *Setd3*$^{-/-}$ and *Setd3*$^{+/+}$ timed-pregnant females. The normal day of birth for *Setd3*$^{+/+}$mice of this strain is 19 d.p.c. All pups born on 18 d.p.c. were removed and euthanized. All mice quantified for fetuses in utero were euthanized at 17:00 on day 19.

A PGF2α cocktail (1 ml Lutalyse (5 mg PGF2α per ml), 1 ml 10% calcium gluconate, 0.05 ml of 50% isotonic dextrose and 8.0 ml of 0.9% sterile saline) was used to induce parturition in two *Setd3*$^{-/-}$ females on 19 d.p.c. Females were injected subcutaneously with 1 ml of the cocktail at three time points on 19 d.p.c. (around 09:00, 12:00 and 17:00). The females were monitored for parturition and euthanized on late 20 d.p.c. at 17:00.

Metabolic analysis. Amino acids were analysed as underivatized compounds by LC–MS/MS. Samples (50 μl) were deproteinized with 50 μl of 6% sulfosalicylic acid and centrifuged for 15 min at 17,000*g*. Supernatants were diluted with an isotopic standard mixture (Cambridge Isotope Laboratories) in 2 μM tridecafluoroheptanoic acid and then injected into the LC–MS/MS system. Samples were analysed using a clinically validated amino acid analysis method[49]. An Agilent 1200 series liquid chromatography system equipped with a Thermo Hypercarb trap column (3 μm, 4.6 mm × 50 mm) and a Waters BEH C18 analytical column (2.5 μm, 2.1 mm × 100 mm) was used to separate compounds in a trap and reverse-elute configuration. An Agilent 6460 triple quadrupole mass spectrometer was used in positive polarity electrospray ionization for detection by dynamic multiple-reaction monitoring. Mobile phase A was 0.02% perfluoroheptanoic acid and mobile phase B was acetonitrile. Standard curves were prepared by diluting amino acid standards (Wako Chemicals); for 1-methyl histidine, *S*-aminoethyl cystine was used as the internal standard and for 3-methyl histidine, histidine-$^{13}C_6{}^{15}N_3$ was used as the internal standard. Agilent Masshunter B08 was used for data analysis.

Muscle tissue histology. Tissues were fixed by immersion in 10% neutral-buffered formalin, processed for paraffin embedding and 5-μm thick sections were stained with haematoxylin and eosin.

Myosin expression and purification. Construction, expression and purification of the wild-type recombinant human β-cardiac myosin sS1 and the hypertrophic cardiac myopathy H251N mutant[50] are described in detail elsewhere[50–52]. In brief, a truncated version of MYH7 (residues 1–808), corresponding to sS1, with a C-terminal enhanced green fluorescent protein (eGFP), was co-expressed with myosin light chain 3 (MYL3), encoding human ventricular essential light chain (ELC) and containing an N-terminal Flag tag (DYKDDDDK) and tobacco etch virus (TEV) protease site in mouse myoblast C2C12 cells using the AdEasy Vector System (Obiogene). The myosin heavy chain with its associated Flag-tagged ELC was first purified from clarified lysate with anti-Flag resin (Sigma-Aldrich). After cleaving off the Flag tag with TEV protease, the human β-cardiac sS1 was further purified using anion exchange chromatography on a 1-ml HiTrap Q HP column (GE Healthcare). Peak fractions were eluted with column buffer (10 mM imidazole pH 7.5, around 200 mM NaCl, 4 mM $MgCl_2$, 1 mM DTT, 2 mM ATP and 10% sucrose) and concentrated by centrifugation in Amicon Ultra-0.5 10-kDa cut-off spin filters (EMD Millipore) before being used in assays or stored at −80 °C.

In vitro motility. Experiments were conducted following previously described methods[52–55]. In brief, frozen myosin proteins were first subjected to a 'deadheading' procedure to remove inactive heads. Myosin was mixed with 5–10× molar excess of unlabelled F-actin on ice for 5 min, followed by addition of 2 mM ATP for 3 min, then centrifuged at 350,000*g* in a TLA-100 rotor (Beckman Coulter) at 4 °C for 20 min. The supernatant was collected for use in the motility. Flow chamber was built on a nitrocellulose-coated coverslip mounted on a glass slide. Deadheaded myosin was immobilized via specific binding to the GFP antibody that non-specifically binds to the coverslip surface, followed by blocking with assay buffer (25 mM imidazole pH 7.5, 25 mM KCl, 4 mM $MgCl_2$, 1 mM EGTA, 10 mM DTT and 1 mg ml^{-1} BSA). A final solution containing fluorescently labelled bovine cardiac F-actin, 2 mM ATP, and an oxygen-scavenging system (0.4% glucose, 0.11 mg ml^{-1} glucose oxidase and 0.018 mg ml^{-1} catalase) was subsequently flowed in before imaging on a total internal reflection fluorescence microscope (Nikon Eclipse Ti-E) equipped with a 561-nm laser (Cobolt) and a 100× oil-immersion objective (Nikon)[56]. Time-lapse movies were acquired at multiple fields of views for each experimental condition at 1 Hz sampling rate. Movies were analysed using the FAST (fast automated spud trekker) software[57] to obtain the mean velocities with 20% tolerance. All experiments were conducted at 23 °C.

Actin-activated myosin ATPase activity. Purified actin was freshly cycled to F-actin by extensive (four times over 4 days) dialysis in ATPase buffer (10 mM imidazole, pH 7.5, 5 mM KCl, 3 mM $MgCl_2$ and 1 mM DTT) to remove any residual ATP. The monomeric concentration of F-actin was determined by measuring the absorbance of a serial dilution of the actin in 6 M guanidine hydrochloride both at 290 nm with an extinction coefficient of 26,600 M^{-1} cm^{-1} and at 280 nm with an extinction coefficient of 45,840 M^{-1} cm^{-1} in a spectrophotometer (NanoDrop). Full-length human gelsolin was added to actin at a ratio of 1:1,000 to reduce the viscosity of the actin and decrease the pipetting error at higher actin concentrations without affecting the ATPase activity. The steady-state actin-activated ATPase activities of freshly prepared human β-cardiac sS1–eGFP myosin using wild-type and knockout actin were determined using a colorimetric readout of phosphate production[58], as described previously[52]. In this assay, reactions containing sS1 at a final concentration of 0.01 mg ml^{-1}, 2 mM ATP and actin at concentrations ranging from 5 to 77 μM were performed at 23 °C with shaking using a microplate spectrophotometer (Thermo Scientific Multiskan GO). The rate of sS1 activity was obtained by linear fitting of the phosphate signal as a function of time and converting to activity units using a phosphate standard. Each actin condition was performed in duplicate. The error on each data point represents the s.e.m. of the duplicates. The Michaelis–Menten equation was fitted to determine the maximal activity (k_{cat}) and the actin concentration at half-maximum (apparent K_m for actin).

Statistics. GraphPad Prism 7.0 and KaldeidaGraph 4.5 were used for statistics.

Reporting summary. Further information on research design is available in the Nature Research Reporting Summary linked to this paper.

Data availability

The X-ray structures (coordinates and structure factor files) of SETD3 with bound actin peptide have been submitted to the PDB under accession numbers 6MBJ ($P2_1$), 6MBK (two complexes in $P2_12_12_1$) and 6MBL (one complex in $P2_12_12_1$). Source Data for this study are provided included in the online version of the paper for Figs. 4d, 5b, e, f, i, k and Extended Data Figs. 7e, 9c, h. Gel source data are provided as Supplementary Fig. 1 for cropped images shown in Fig. 1a–e, 2a, c, 3a–g, 4c, 5g, j and Extended Data Fig. 1b. Mass spectrometry data associated with Fig. 1c and Extended Data Fig. 1h are provided in Supplementary Tables 1. Mass spectrometry data associated with Fig. 3i are provided in Supplementary Tables 2. Additional requests for data can be made to the corresponding authors.

22. Kwiatkowki, S. et al. SETD3 protein is the actin-specific histidine *N*-methyltransferase. *eLife* **7**, e37921 (2018).
23. Rothbart, S. B., Krajewski, K., Strahl, B. D. & Fuchs, S. M. Peptide microarrays to interrogate the "histone code". *Methods Enzymol.* **512**, 107–135 (2012).
24. Patel, A., Dharmarajan, V., Vought, V. E. & Cosgrove, M. S. On the mechanism of multiple lysine methylation by the human mixed lineage leukemia protein-1 (MLL1) core complex. *J. Biol. Chem.* **284**, 24242–24256 (2009).
25. Edmunds, J. W., Mahadevan, L. C. & Clayton, A. L. Dynamic histone H3 methylation during gene induction: HYPB/Setd2 mediates all H3K36 trimethylation. *EMBO J.* **27**, 406–420 (2008).
26. An, S., Yeo, K. J., Jeon, Y. H. & Song, J. J. Crystal structure of the human histone methyltransferase ASH1L catalytic domain and its implications for the regulatory mechanism. *J. Biol. Chem.* **286**, 8369–8374 (2011).
27. Chuikov, S. et al. Regulation of p53 activity through lysine methylation. *Nature* **432**, 353–360 (2004).
28. Feng, Q. et al. Methylation of H3-lysine 79 is mediated by a new family of HMTases without a SET domain. *Curr. Biol.* **12**, 1052–1058 (2002).
29. Huang, J. et al. Repression of p53 activity by Smyd2-mediated methylation. *Nature* **444**, 629–632 (2006).
30. Rea, S. et al. Regulation of chromatin structure by site-specific histone H3 methyltransferases. *Nature* **406**, 593–599 (2000).
31. Tachibana, M., Sugimoto, K., Fukushima, T. & Shinkai, Y. Set domain-containing protein, G9a, is a novel lysine-preferring mammalian histone methyltransferase with hyperactivity and specific selectivity to lysines 9 and 27 of histone H3. *J. Biol. Chem.* **276**, 25309–25317 (2001).
32. Kuo, A. J. et al. NSD2 links dimethylation of histone H3 at lysine 36 to oncogenic programming. *Mol. Cell* **44**, 609–620 (2011).
33. Mazur, P. K. et al. SMYD3 links lysine methylation of MAP3K2 to Ras-driven cancer. *Nature* **510**, 283–287 (2014).
34. Fang, J. et al. Purification and functional characterization of SET8, a nucleosomal histone H4-lysine 20-specific methyltransferase. *Curr. Biol.* **12**, 1086–1099 (2002).
35. Kurash, J. K. et al. Methylation of p53 by Set7/9 mediates p53 acetylation and activity in vivo. *Mol. Cell* **29**, 392–400 (2008).
36. Levy, D. et al. Lysine methylation of the NF-κB subunit RelA by SETD6 couples activity of the histone methyltransferase GLP at chromatin to tonic repression of NF-κB signaling. *Nat. Immunol.* **12**, 29–36 (2011).
37. Baymaz, H. I., Spruijt, C. G. & Vermeulen, M. Identifying nuclear protein–protein interactions using GFP affinity purification and SILAC-based quantitative mass spectrometry. *Methods Mol. Biol.* **1188**, 207–226 (2014).
38. Hsiao, K., Zegzouti, H. & Goueli, S. A. Methyltransferase-Glo: a universal, bioluminescent and homogenous assay for monitoring all classes of methyltransferases. *Epigenomics* **8**, 321–339 (2016).
39. Cox, J. & Mann, M. MaxQuant enables high peptide identification rates, individualized p.p.b.-range mass accuracies and proteome-wide protein quantification. *Nat. Biotechnol.* **26**, 1367–1372 (2008).
40. Kron, S. J., Drubin, D. G., Botstein, D. & Spudich, J. A. Yeast actin filaments display ATP-dependent sliding movement over surfaces coated with rabbit muscle myosin. *Proc. Natl Acad. Sci. USA* **89**, 4466–4470 (1992).
41. Schafer, D. A., Jennings, P. B. & Cooper, J. A. Rapid and efficient purification of actin from nonmuscle sources. *Cell Motil. Cytoskeleton* **39**, 166–171 (1998).
42. Otwinowski, Z., Borek, D., Majewski, W. & Minor, W. Multiparametric scaling of diffraction intensities. *Acta Crystallogr. A* **59**, 228–234 (2003).
43. McCoy, A. J. et al. Phaser crystallographic software. *J. Appl. Crystallogr.* **40**, 658–674 (2007).
44. Afonine, P. V. et al. Towards automated crystallographic structure refinement with phenix.refine. *Acta Crystallogr. D* **68**, 352–367 (2012).
45. Emsley, P. & Cowtan, K. Coot: model-building tools for molecular graphics. *Acta Crystallogr. D* **60**, 2126–2132 (2004).
46. Hansen, S. D., Zuchero, J. B. & Mullins, R. D. Cytoplasmic actin: purification and single molecule assembly assays. *Methods Mol. Biol.* **1046**, 145–170 (2013).
47. Yao, X., Nguyen, V., Wriggers, W. & Rubenstein, P. A. Regulation of yeast actin behavior by interaction of charged residues across the interdomain cleft. *J. Biol. Chem.* **277**, 22875–22882 (2002).
48. Bradley, A. et al. The mammalian gene function resource: the International Knockout Mouse Consortium. *Mamm. Genome* **23**, 580–586 (2012).
49. Le, A., Ng, A., Kwan, T., Cusmano-Ozog, K. & Cowan, T. M. A rapid, sensitive method for quantitative analysis of underivatized amino acids by liquid chromatography–tandem mass spectrometry (LC–MS/MS). *J. Chromatogr. B Analyt. Technol. Biomed. Life Sci.* **944**, 166–174 (2014).
50. Adhikari, A. S. et al. Early-onset hypertrophic cardiomyopathy mutations significantly increase the velocity, force, and actin-activated atpase activity of human β-cardiac myosin. *Cell Rep.* **17**, 2857–2864 (2016).
51. Sommese, R. F. et al. Molecular consequences of the R453C hypertrophic cardiomyopathy mutation on human β-cardiac myosin motor function. *Proc. Natl Acad. Sci. USA* **110**, 12607–12612 (2013).
52. Liu, C., Kawana, M., Song, D., Ruppel, K. M. & Spudich, J. A. Controlling load-dependent kinetics of β-cardiac myosin at the single-molecule level. *Nat. Struct. Mol. Biol.* **25**, 505–514 (2018).
53. Kron, S. J., Toyoshima, Y. Y., Uyeda, T. Q. & Spudich, J. A. Assays for actin sliding movement over myosin-coated surfaces. *Methods Enzymol.* **196**, 399–416 (1991).
54. Nag, S. et al. Contractility parameters of human β-cardiac myosin with the hypertrophic cardiomyopathy mutation R403Q show loss of motor function. *Sci. Adv.* **1**, e1500511 (2015).
55. Kawana, M., Sarkar, S. S., Sutton, S., Ruppel, K. M. & Spudich, J. A. Biophysical properties of human β-cardiac myosin with converter mutations that cause hypertrophic cardiomyopathy. *Sci. Adv.* **3**, e1601959 (2017).
56. Mortensen, K. I., Sung, J., Flyvbjerg, H. & Spudich, J. A. Optimized measurements of separations and angles between intra-molecular fluorescent markers. *Nat. Commun.* **6**, 8621 (2015).
57. Aksel, T., Choe Yu, E., Sutton, S., Ruppel, K. M. & Spudich, J. A. Ensemble force changes that result from human cardiac myosin mutations and a small-molecule effector. *Cell Rep.* **11**, 910–920 (2015).
58. Trybus, K. M. Biochemical studies of myosin. *Methods* **22**, 327–335 (2000).

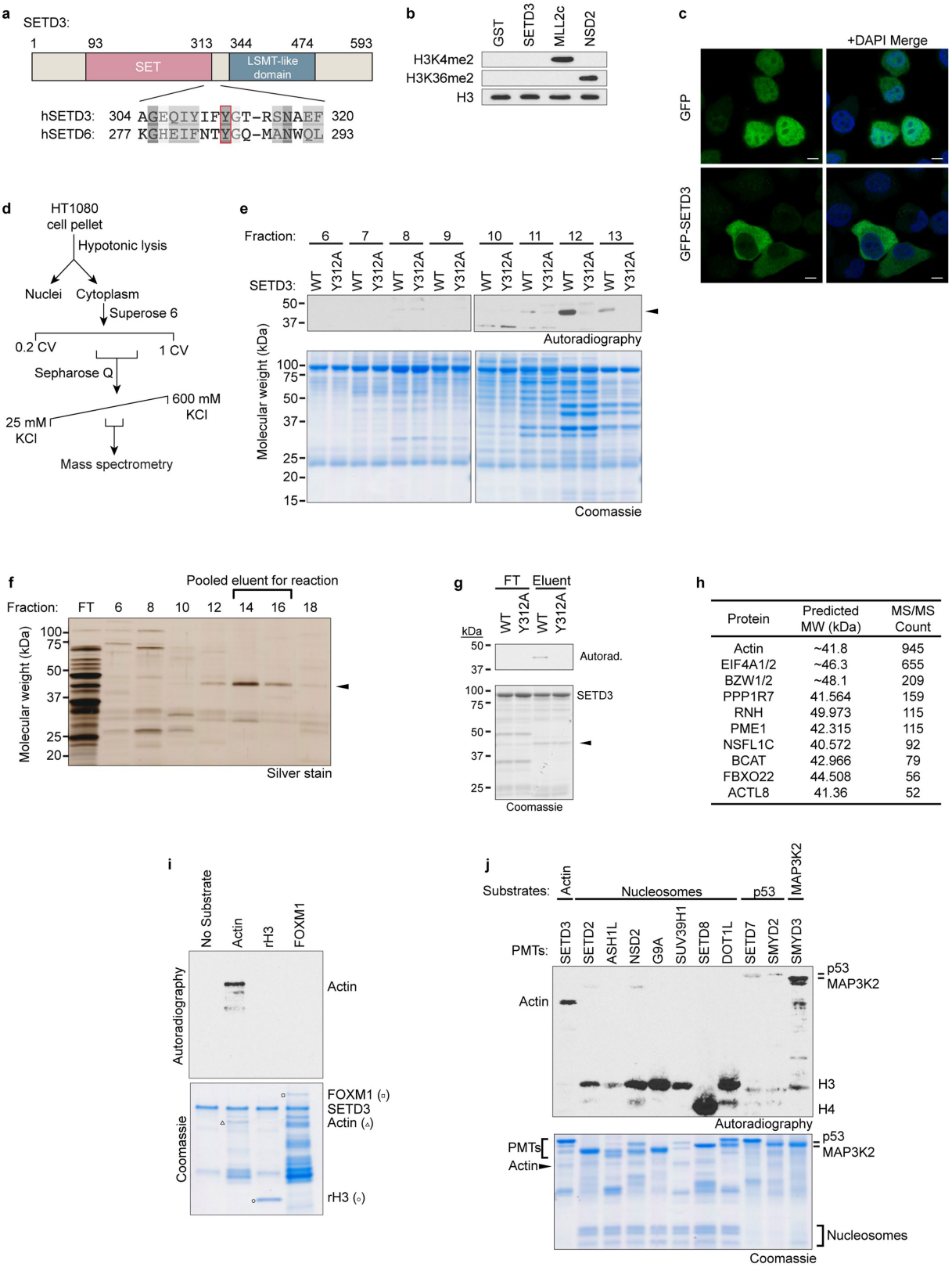

Extended Data Fig. 1 | See next page for caption.

Extended Data Fig. 1 | Identification of actin as a SETD3 substrate. **a**, Top, domain structure of SETD3 containing an N-terminal SET domain and a C-terminal domain homologous to plant Rubisco LSMT. Bottom, alignment of the homologous methyltransferases human SETD3 and human SETD6. Red box, putative catalytic tyrosine. **b**, Methylation reactions as in Fig. 1a with non-radiolabelled SAM and analysed by western blot with indicated antibodies. Total histone H3 is shown as a loading control. **c**, SETD3 localizes to the cytoplasm. Representative immunofluorescence images of GFP or GFP–SETD3 localization in HeLa cells (left) are merged with DAPI counterstaining (right). Scale bars, 7 μm. **d**–**g**, Biochemical enrichment of a candidate SETD3 substrate. **d**, Schematic of biochemical strategy to identify the methylated band indicated in Fig. 1b. **e**, In vitro methylation reactions using cell extracts separated by size-exclusion chromatography as a substrate. Reactions were performed with either wild-type (WT) SETD3 or a putative catalytic mutant (Y312A). Reactions were analysed as in Fig. 1. Arrowhead, candidate substrate. **f**, Ion-exchange chromatography separates candidate substrates. Fractions positive for SETD3-specific methylation by size-exclusion chromatography were further separated by ion-exchange chromatography and either the flow through (FT) or the pooled fractions containing a notable silver-stained band (arrowhead) at the size of the candidate substrate were used as substrate in an in vitro methylation reaction. **g**, Flow through or pooled eluent from ion-exchange chromatography were used as substrate for methylation reactions as in **e**. Arrowhead, protein band in eluent that was analysed by mass spectrometry. **h**, Top candidate substrates with molecular weights (MW) that were similar to the size of the SETD3-dependent band from in vitro reactions with cell extracts. Candidates identified by mass spectrometry are ranked by abundance determined by MS/MS count (Supplementary Table 1). **i**, In vitro methylation reactions with SETD3 on actin, recombinant histone H3 (rH3), FOXM1 or a no substrate as a control. Top, ^{3}H-SAM is the methyl donor and methylation visualized by autoradiography. Bottom, Coomassie staining of proteins in the reaction. **j**, In vitro methylation reactions with the indicated enzymes and substrates. All experiments were repeated at least three times with similar results.

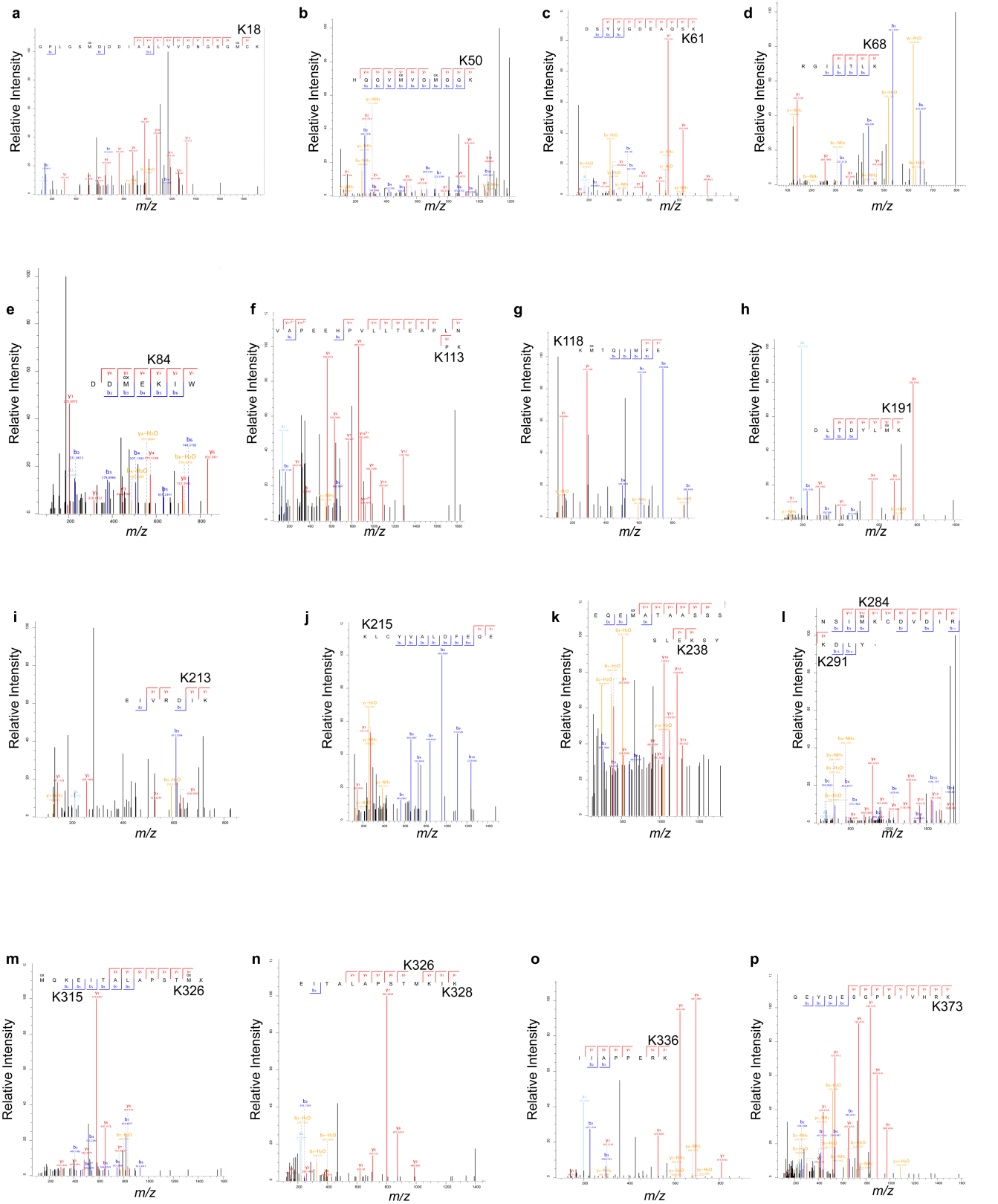

Extended Data Fig. 2 | SETD3 does not methylate β-actin lysines. GST–β-actin was expressed in bacteria, and cleaved using PreScission Protease. Cleaved β-actin was used in an in vitro methylation assay with SETD3 and deuterated SAM. Spectra are representative of experiments independently performed three times with similar results. MS/MS spectra with identified ions for unmethylated lysine residues produced with indicated proteases. **a**, K18 (trypsin) (identified N-terminal GPLGS amino acids are residual, vector-specific amino acids from the original GST fusion protein). **b**, Lys50 (trypsin). **c**, Lys61 (trypsin). **d**, Lys68 (trypsin). **e**, Lys84 (chymotrypsin). **f**, Lys113 (trypsin). **g**, Lys118 (Glu-C). **h**, Lys191 (trypsin). **i**, Lys213 (trypsin). **j**, Lys215 (Glu-C). **k**, Lys238 (chymotrypsin). **l**, Lys284/K291 (chymotrypsin). **m**, Lys315 and Lys326 (trypsin). **n**, Lys326 and Lys328 (trypsin). **o**, Lys336 (trypsin). **p**, Lys373 (trypsin).

a

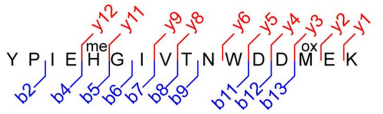

Ions	-SETD3 *m/z*	+SETD3 *m/z*	Ions	-SETD3 *m/z*	+SETD3 *m/z*
b2	261.122	261.122	y1	147.113	147.113
b4	503.248	–	y2	276.156	276.156
b5*	640.304	657.343	y3	423.192	423.189
b6*	697.331	714.369	y4	538.218	538.220
b7*	810.411	827.442	y5	653.245	653.243
b8*	909.479	926.508	y6	839.324	–
b9*	–	1027.579	y8	1054.409	–
b11*	1310.629	–	y9	–	1153.498
b12*	1425.675	1442.700	y11	1323.581	1323.581
b13*	1540.690	1557.712	y12*	1460.633	1477.681

Deuterated methyl = +17.03 Da

b

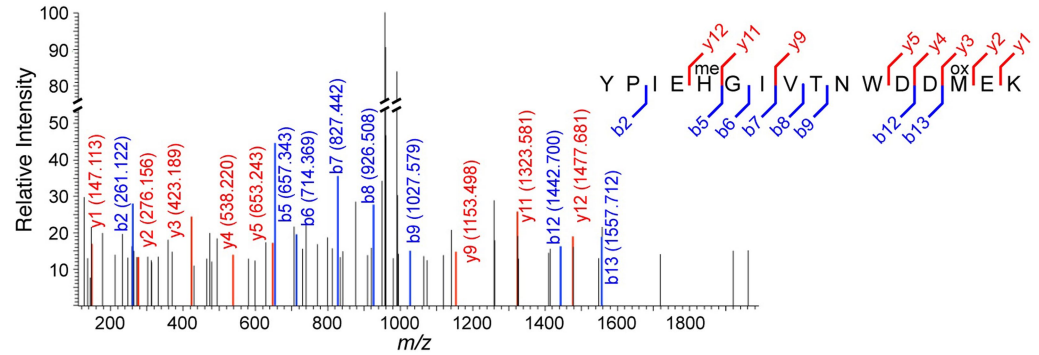

c

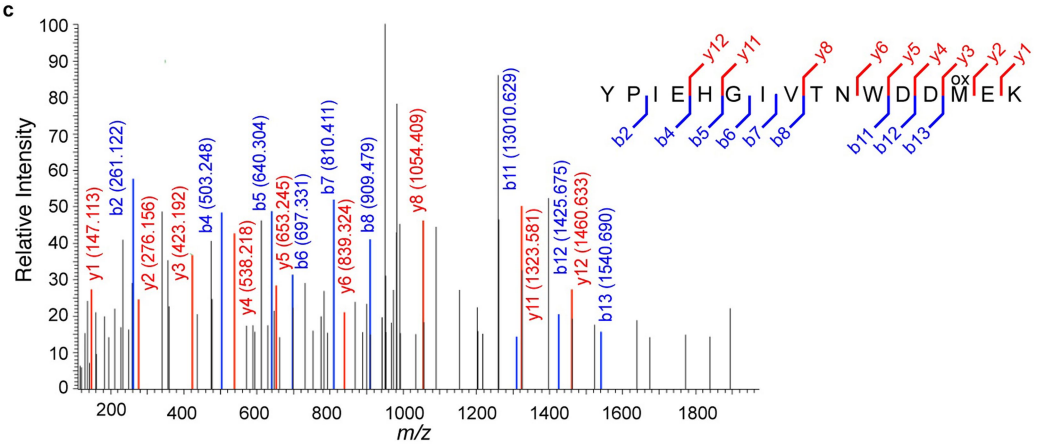

d

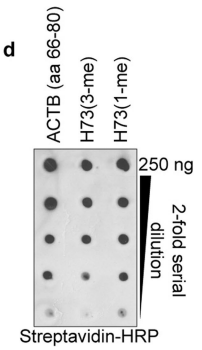

e

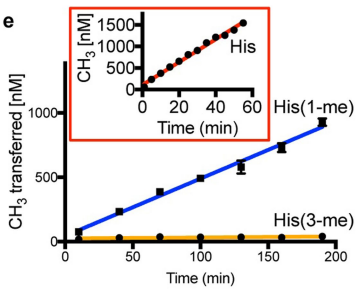

f

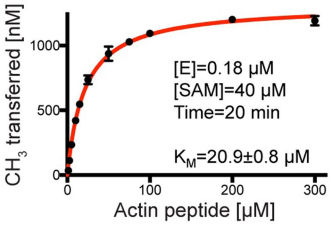

g

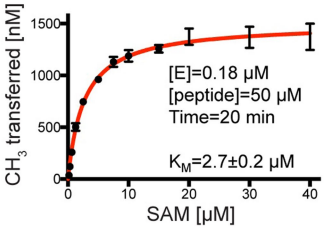

Extended Data Fig. 3 | See next page for caption.

Extended Data Fig. 3 | SETD3 generates actin-His73(3-me). a–**c**, MS/MS identifies His73 of actin as a SETD3-methylated residue. **a**, Top, methylated tryptic peptide with indicated *b* and *y* ions. Modifications: me, methylation; ox, oxidation. Bottom, *m*/*z* for *b* and *y* ions identified in MS/MS spectra from methylation reactions with (+SETD3) or without (−SETD3) using deuterated SAM as the methyl donor (+17.03 Da mass shift). Peptides containing His73 are indicated by an asterisk. **b**, **c**, In vitro methylation reactions with (**b**) and without (**c**, negative control) SETD3 and β-actin with deuterated SAM were analysed by mass spectrometry. Left, MS/MS spectra of tryptic peptides containing His73. Right, *b* and *y* ions identified from oxidized peptides in each spectrum are indicated. **d**, Dot blot loading control for Fig. 2c of biotinylated ACTB peptides (amino acids 66–80) that are unmodified at His73 or methylated in the N3 (3-me) or N1 (1-me) position. Serial dilutions of the peptides were visualized by streptavidin–HRP and chemiluminescence. **e**–**g**, Methylation reaction kinetics for SETD3 and the actin peptide. **e**, Time course of SETD3 with His(1-me) or His(3-me) modified peptides as substrate. Inset, unmodified peptide using 80-fold lower enzyme concentrations compared to the concentrations used for modified peptides. **f**, **g**, Steady-state kinetics of SETD3 for the human β-actin peptide (residues 66–80) (**f**) and SAM (**g**). Kinetic measurements were performed using a bioluminescence methyltransferase assay, MTase-Glo (Promega). Data are mean ± s.d. of biological triplicates for each data point. **a**–**g**, Data are representative of three independent experiments with similar results.

a

Organism	% methyl
S. cerevisiae	N.D.
A. thaliana	9%
N. benthamiana	17%
C. elegans	98%
D. melanogaster	97%
S. frugiperda	90%
D. rerio	98%
X. laevis	98%
G. gallus	98%
M. musculus	98%
H. sapiens	97%

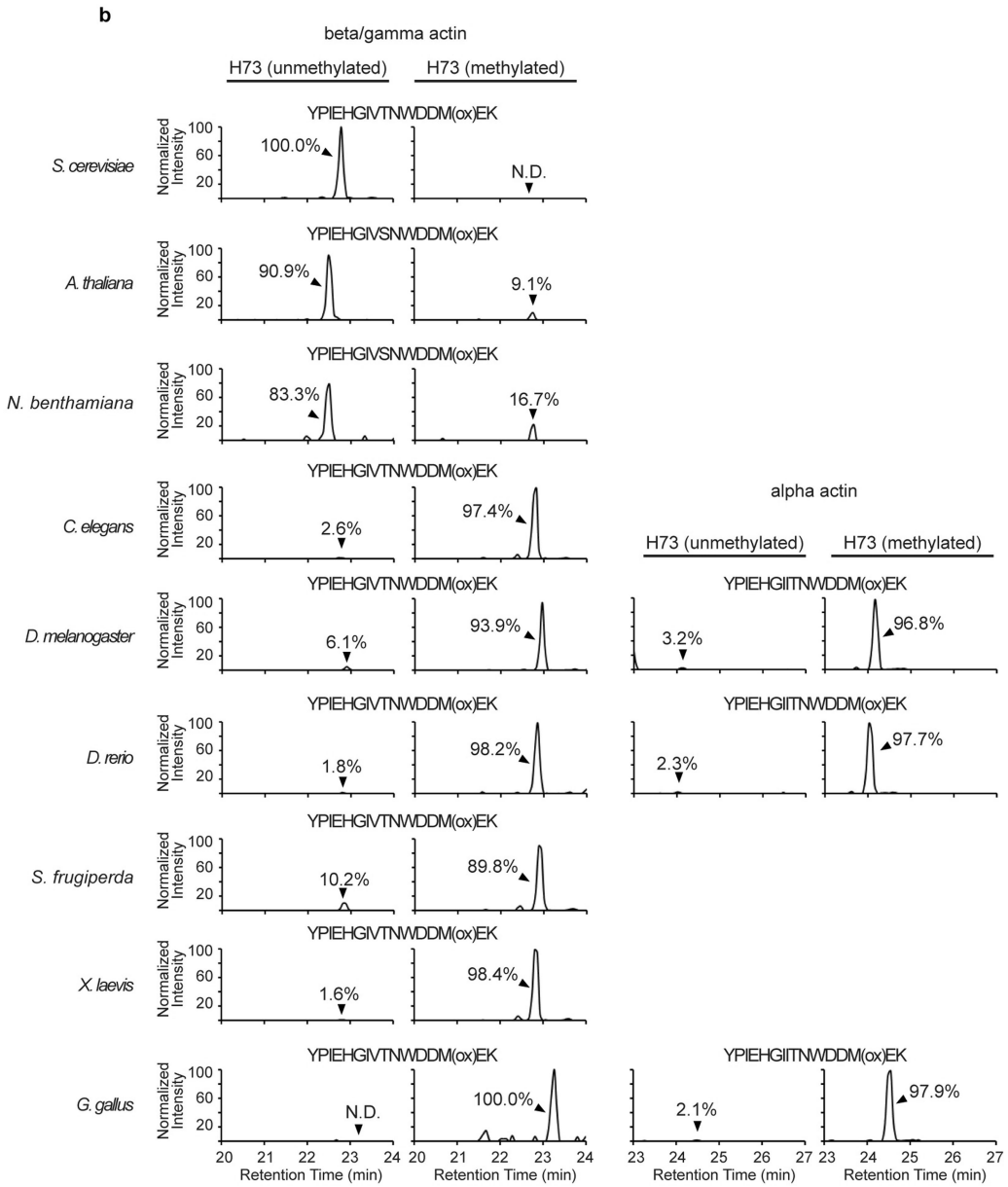

Extended Data Fig. 4 | Methylation of the conserved actin-His73 residue is present in diverse organisms. a, Summary of actin histidine methylation on the conserved His73 residue among model organisms. Abundance of methylation is reported as a percentage of peptide that is methylated. **b**, Chromatograms of MH^{3+} ions ($m/z \pm 10$ p.p.m.) for methylated and unmethylated versions of the indicated peptides. The unmethylated actin peptide that was analysed for each species is shown above the corresponding chromatograms. When α-actin peptides were detected, associated chromatograms and quantification are provided on the right. The area of indicated peaks was normalized to the sum of the area between peptides (with or without methylation) and the percentage abundance is labelled. Chromatograms that quantify actin histidine methylation in human and mouse can be found in Extended Data Figs. 6, 7. N.D., not detected. Quantification represents data from two independent experiments with similar results.

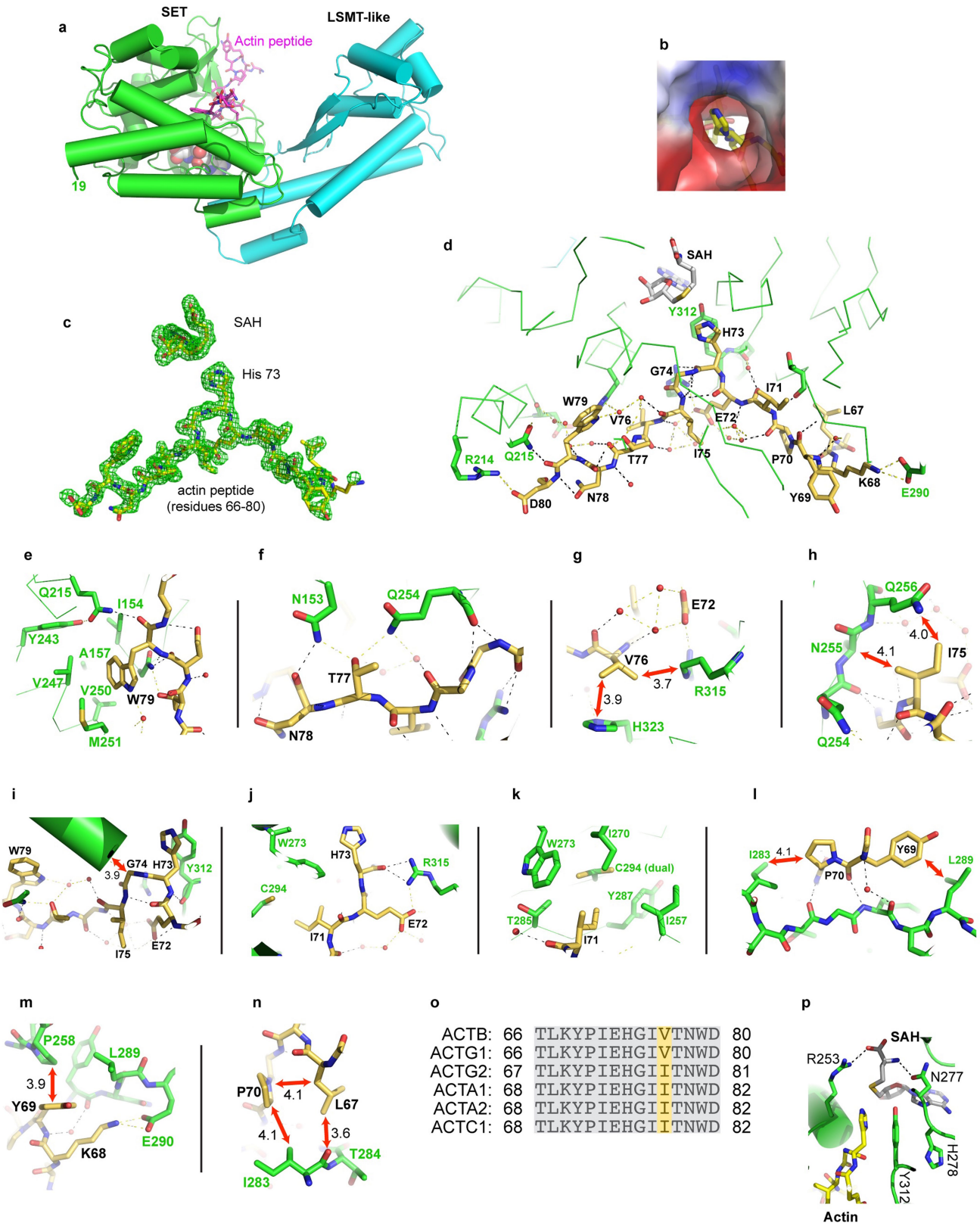

Extended Data Fig. 5 | See next page for caption.

Extended Data Fig. 5 | Structural details of SETD3–actin peptide interactions. a, Overall structure of SETD3 with a V-shaped cleft constructed by the SET domain (green) and an LSMT-like domain (cyan). Helices are shown as cylinders and strands as arrows. The actin peptide is shown as a stick model. **b**, View of the target histidine through the channel from the SAH-binding pocket. **c**, Omit electron density of F_o–F_c, contoured at 3.0σ above the mean, is shown for omitting cofactor SAH and the actin peptide used for co-crystallization. **d**, Details of inter- and intramolecular interactions between SETD3 (green) and actin peptide (yellow). **e**, Trp79 of actin bound in a hydrophobic surface pocket of SETD3. **f**, Thr77 and Asn78 of actin form hydrogen bonds with Asn153 and Gln254 of SETD3. **g**, Val76 of actin is in van der Waals contact with SETD3 residues His323 and Arg315, which in turn interacts with Glu72 of actin. **h**, Ile75 of actin is in van der Waals contact with main-chain C_α of Asn255 and Gln256 of SETD3. **i**, Gly74 of actin is located in the amino end of a SETD3 helix. The imidazole ring of His73 (the substrate target) is parallel with the aromatic ring of Tyr312 of SETD3. **j**, SETD3 Arg315 bridges between the carboxylate oxygen of Glu72 and the main-chain carbonyl oxygen of His73 of actin. **k**, Ile71 of actin is accommodated in a surface hydrophobic pocket of SETD3. **l**, Tyr69 and Pro70 of actin interact with a stretch of SETD3 residues from Ile283 to Leu289. **m**, Tyr69 of actin packs against Pro258 of SETD3 and Lys68 of actin interacts with Glu290 of SETD3. **n**, Leu67 and Pro70 of actin form an intramolecular interaction and both interact with Ile283 and Thr284 of SETD3. **o**, Alignment of the amino acids from all six human actin isoforms corresponding to β-actin amino acids 66–80. Variant amino acids are highlighted in yellow. **p**, The cofactor (SAH) binding site includes residues Arg253, Tyr312, Asn277 and His278 of SETD3.

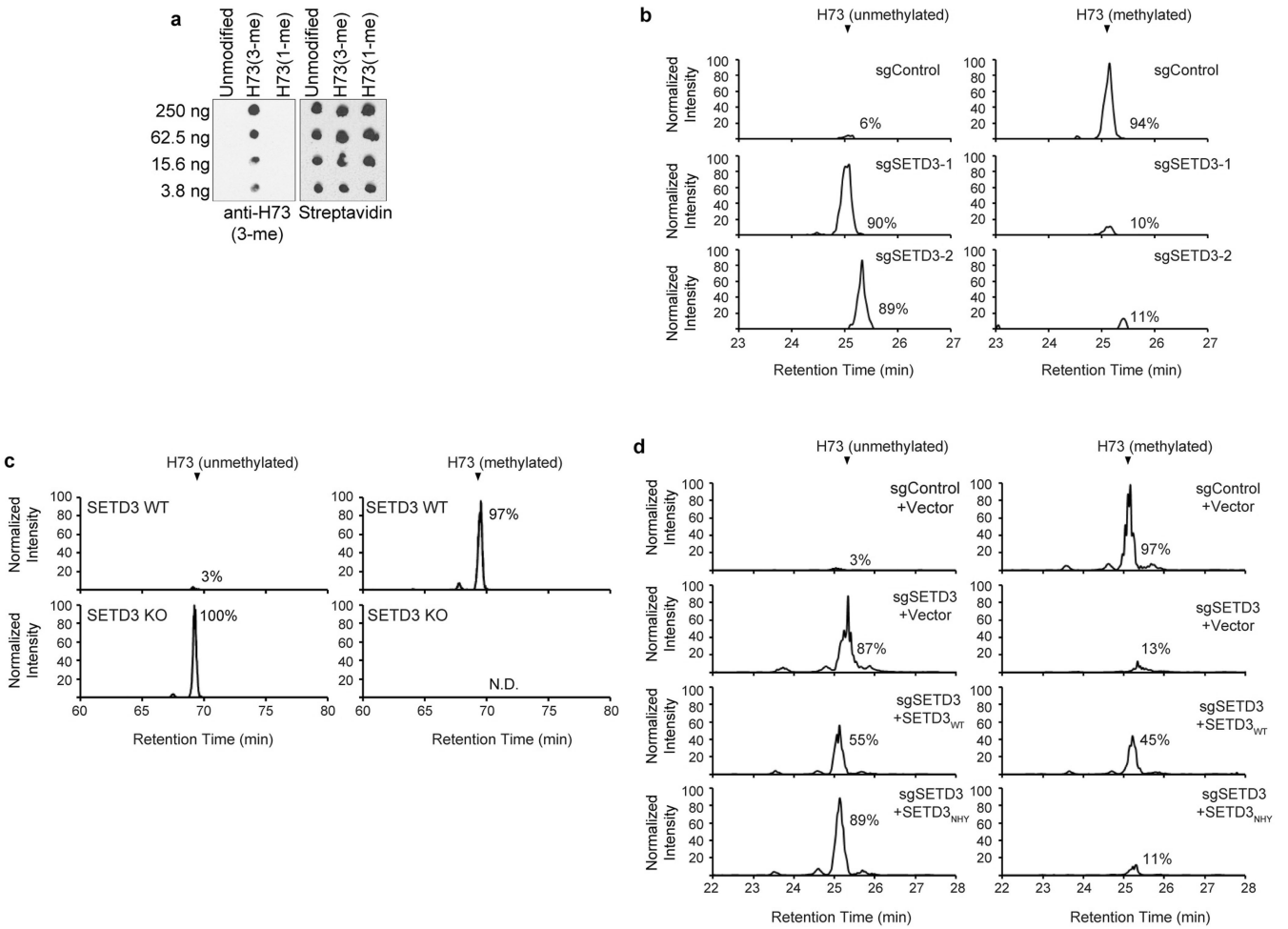

Extended Data Fig. 6 | SETD3 is required for actin methylation in cells. a, Peptide dot blot spotted with biotinylated β-actin peptides (amino acids 66–80) containing His73, His73(3-me) or His73(1-me). Blots were probed with a His73(3-me)-specific antibody or streptavidin as a loading control. **b**–**d**, Chromatograms for quantification of actin-His73me in human cells. Stoichiometry of oxidized β/γ-actin His73 peptide (YPIEHGIVTNWDDM(ox)EK) with and without methylation after purification from cells. MH^{3+} *m*/*z*: unmethylated, 654.968 ± 10 p.p.m.; methylated, 659.6401 ± 10 p.p.m. α-Actin peptide was not detected in these cells. Quantification performed as in Extended Data Fig. 4. **b**, Chromatograms of HT1080 cells treated with CRISPR–Cas9 that is targeted with a control sgRNA or *SETD3*-specific sgRNAs. **c**, Chromatograms of actin His73 methylation in wild-type HeLa cells or clonal HeLa *SETD3* knockout cells. N.D., not detected. **d**, Chromatograms of actin His73 methylation in HT1080 cells treated with CRISPR–Cas9 targeted with either a control or *SETD3*-specific sgRNA and complemented with CRISPR-resistant SETD3(WT), SETD3(NHY) or control plasmids. Experiments were independently performed three times with similar results.

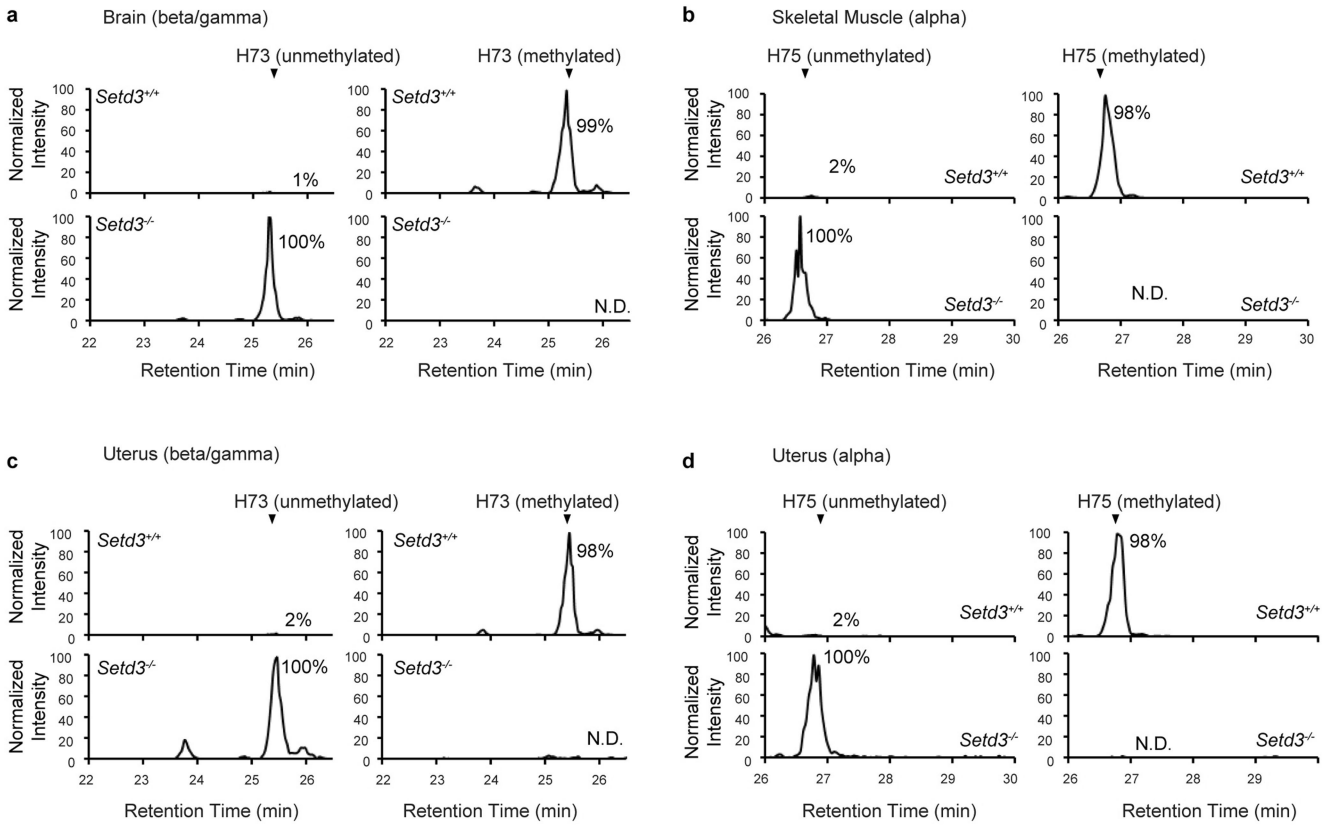

e

Amino Acid	Relative abundance KO/(WT+HET)
Histidine	0.935 ± 0.096
1-Methylhistidine	0.834 ± 0.104
3-Methylhistidine*	0.221 ± 0.076
Alanine	0.804 ± 0.183
Arginine	0.749 ± 0.106
Asparagine	0.867 ± 0.137
Aspartic Acid	0.785 ± 0.158
Glutamic Acid	0.861 ± 0.130
Glutamine	0.892 ± 0.065
Glycine	0.916 ± 0.072
Isoleucine	0.891 ± 0.136
Leucine	0.866 ± 0.142
Lysine	0.657 ± 0.210
Methionine	0.801 ± 0.143
Phenylalanine	1.002 ± 0.101
Proline	0.767 ± 0.187
Serine	0.871 ± 0.120
Threonine	0.821 ± 0.188
Tryptophan	0.799 ± 0.115
Tyrosine	0.991 ± 0.117
Valine	0.904 ± 0.118

Extended Data Fig. 7 | SETD3 is required for actin-His73 methylation in mice. a–**d**, Chromatograms for the quantification of actin histidine methylation in mouse tissues. **a**, Chromatograms to determine the abundance of histidine methylation of the β/γ-actin His73 peptide (YPIEHGIVTNWDDM(ox)EK) with and without methylation after purification from brain tissue of mice with the indicated genotypes. MH^{3+} *m*/*z*: unmethylated, 654.968 ± 10 p.p.m.; methylated, 659.640 ± 10 p.p.m. α-Actin peptide was not detected in these cells. Quantification performed as in Extended Data Fig. 4. **b**, Chromatograms to determine the abundance of histidine methylation on α-actin H75 peptide (YPIEHGIITNWDDM(ox)EK) from skeletal muscle as in **a**. MH^{3+} *m*/*z*: unmethylated, 659.640 ± 10 p.p.m.; methylated, 664.312 ± 10 p.p.m. The β/γ-actin peptide was not detected in these cells. **c**, Chromatograms to determine the abundance of β/γ-actin His73 methylation from uterine tissue as in **a**. **d**, Chromatograms to determine the abundance of α-actin H75 methylation from uterine tissue as in **b**. Quantification was independently performed three times with similar results. **e**, Quantitative amino acid panel from mouse blood serum. Quantitative profiling of amino acids in plasma is used clinically to diagnose metabolic disorders. 3-methyl histidine (indicated by an asterisk) is one of the amino acids measured in the panel, and actin is thought to be the primary source of this metabolite. Amino acid levels from $Setd3^{-/-}$ (KO, $n = 8$) mice were normalized to levels of amino acids from animals with normal His73 methylation levels (total, $n = 12$; $Setd3^{+/+}$ (WT), $n = 5$; $Setd3^{+/-}$ (HET), $n = 7$). Standard error of the difference between two means is shown for the indicated *n*.

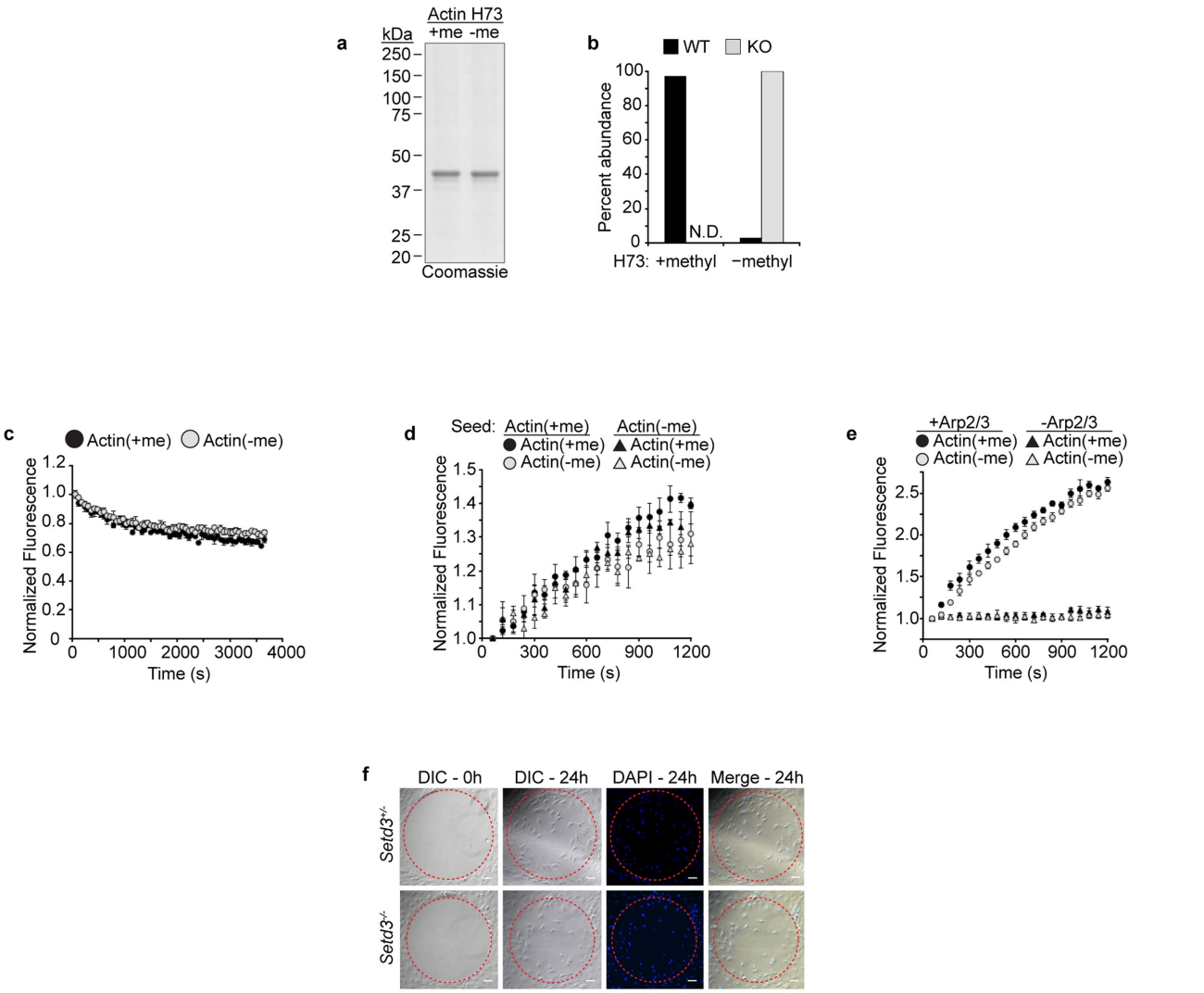

Extended Data Fig. 8 | SETD3-dependent actin-His73 methylation modestly regulates polymerization. a, **b**, Purification of actin with and without His73 methylation. **a**, Coomassie-stained gel of the actin purified from HeLa cell lines described in Fig. 3f for actin(+me) or actin(−me), and used in the biochemical assays described in Fig. 4a, b and in **c**–**e**. **b**, Mass spectrometry quantification of actin His73 methylation from **a**. Representative data from an experiment performed at least three times with similar results. **c**, Methylation does not alter actin depolymerization rates. Actin polymerized as in Fig. 4a was diluted to 0.02 μM and depolymerization was monitored by fluorescence normalized to initial values. **d**, Elongation of the indicated monomeric actin (1 μM, 0.1 μM pyrene–actin) measured in the presence of 2 μM phalloidin–actin seeds made with methylated (circles) or unmethylated (triangles) actin. **e**, Arp2/3 complex-induced actin polymerization performed in the presence of 100 nM WASP VCA and 5 nM Arp2/3 complex with 1 μM of the indicated monomeric actin and 0.1 μM pyrene–actin. **c**–**e**, Mean values plotted with s.e.m. from three independent biological replicates. **f**, SETD3 promotes cell migration. Representative images of cell migration assays performed three times with similar results using cells from Fig. 4c. A circular void of cells was created at the start of the assay (0 h, dashed red circle). After 24 h of migration, cells were fixed and stained with DAPI. Scale bars, 100 μm.

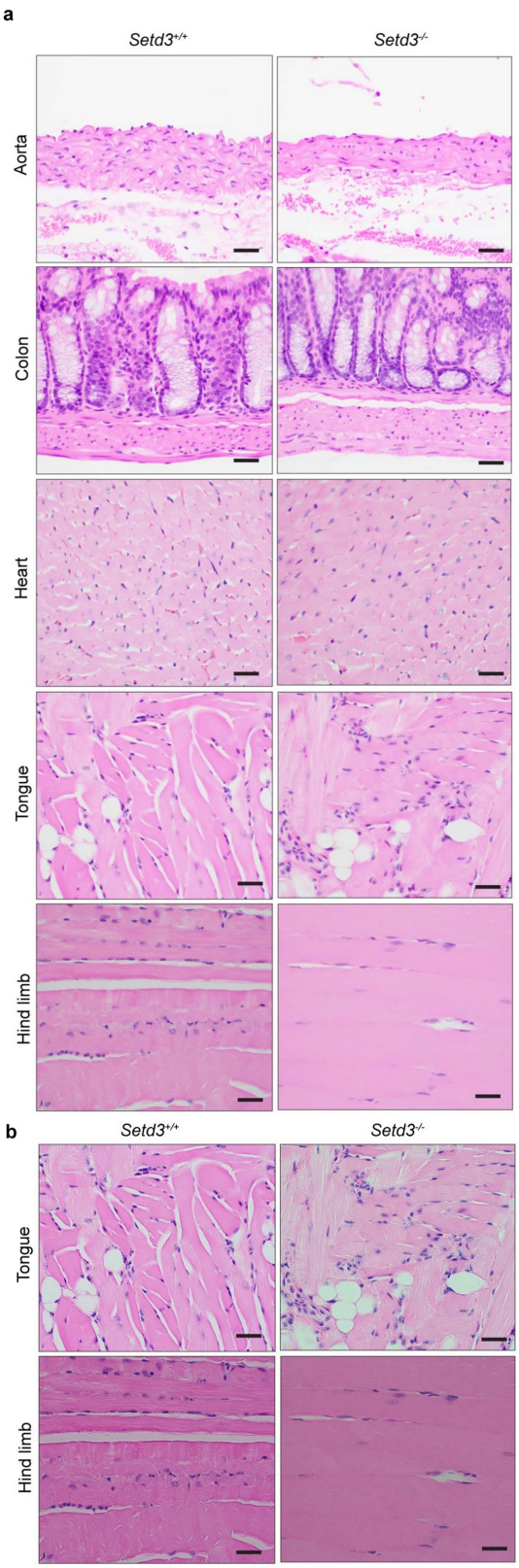

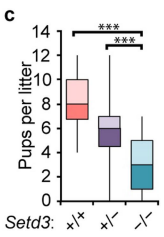

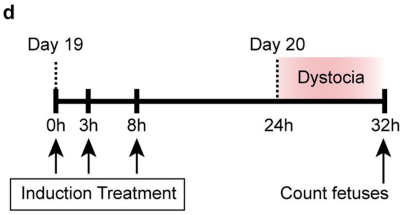

e

Genotype	Day 19 Births	Day 20 Births	Postterm Fetuses *in utero*
+/+	10	0	0
+/−	8	0	0
−/−	0	1	7
−/−	0	1	10

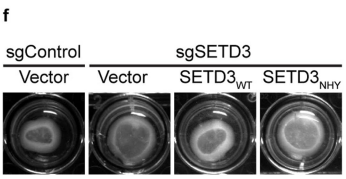

g

		Mean Filtered Velocity (nm/s)	
		Actin(+me)	Actin(-me)
Myosin	sS1-WT	737 ± 2	777 ± 8
	sS1-H251N	1054 ± 4	1108 ± 6

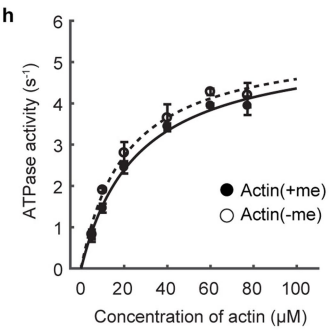

Extended Data Fig. 9 | See next page for caption.

Extended Data Fig. 9 | Analysis of SETD3 and actin-His73me in parturition and uterine smooth muscle contraction. a, **b**, Histology of muscle tissues from *Setd3*$^{+/+}$ and *Setd3*$^{-/-}$ mice. **a**, Haematoxylin and eosin staining of aorta, colon, heart, tongue and hind limb muscle from *Setd3*$^{+/+}$ and *Setd3*$^{-/-}$ mice. **b**, Tongue and hind limb (striated muscle) sections from **a** were re-imaged without a condenser to highlight the sarcoplasmic striations characteristic of this muscle type. Scale bars, 20 μm. Images from three independent experiments gave similar results. **c**, Quantification of pups per litter for *Setd3*$^{+/+}$ ($n = 12$), *Setd3*$^{+/-}$ ($n = 43$), *Setd3*$^{-/-}$ ($n = 26$) mothers. ***P value ≤ 0.001. **d**, **e**, Labour induction at 19 d.p.c. does not rescue dystocia of *Setd3*$^{-/-}$ pregnant mice. **d**, Schematic of prostaglandin treatment protocol. The PGF2α cocktail was administered at 0, 3 and 8 h on day 19 with euthanasia and quantification of fetuses at 32 h after the first treatment. **e**, Quantification of the births and post-term fetuses in utero for the indicated genotypes at the time shown in the schematic. Note: controls delivered before treatment commenced. **f**, Collagen contraction assay as in Fig. 5h with indicated reconstitution cell lines from Fig. 5j performed with three independent biological replicates. **g**, **h**, Actin-His73me does not notably alter myosin activity. **g**, In vitro actin motility assay. Gliding velocities of actin filaments prepared from actin described in Fig. 4 were measured using human β-cardiac sS1 myosin or a hyperactive mutant (H251N). Data are mean ± s.e.m. velocities from four different experiments. **h**, Actin-activated ATPase of human β-cardiac sS1 using actin as in **g**. The Michaelis–Menten equation was fitted to the ATPase data for wild-type actin (solid line) and knockout actin (dashed line). Points are means from two independent experiments. For gel source data, see Supplementary Fig. 1.

Extended Data Table 1 | Summary of X-ray data collection from the SER-CAT beamline (22-ID) at a wavelength of 1 Å and refinement statistics

SETD3	Actin peptide SAH	Actin peptide SAH	Actin peptide SAH
PDB Code	6MBJ	6MBK	6MBL
Data Collection			
Space group	$P2_1$	$P2_12_12_1$	$P2_12_12_1$
Cell dimensions (Å)	60.35, 176.17, 66.58	60.28, 115.97, 173.59	56.56, 92.83, 111.64
α, β, γ (°)	90, 92.9, 90	90, 90, 90	90, 90, 90
Resolution (Å)	39.07-1.79 (1.85-1.79)	39.38-1.69 (1.75-1.69)	48.30-2.19 (2.27-2.19)
R_{merge}	0.146 (0.892)	0.129 (0.800)	0.125 (0.741)
R_{pim}	0.041 (0.436)	0.061 (0.592)	0.066 (0.548)
$CC_{1/2}$, CC	(0.463, 0.795)	(0.720, 0.915)	(0.402, 0.757)
<I/σI>	14.5 (1.0)	11.3 (1.7)	14.1 (1.5)
Completeness (%)	94.5 (78.9)	99.2 (98.4)	99.5 (96.7)
Redundancy	13.6 (8.0)	19.2 (8.9)	10.6 (4.7)
Observed reflections	1,695,347	2,597,462	323,060
Unique reflections	124,387 (10,380)	135,382 (13,262)	30,434 (2920)
Refinement			
Resolution (Å)	1.79	1.69	2.19
No. reflections	123,743	135,110	30,334
R_{work} / R_{free}	0.199 / 0.223	0.228 / 0.243	0.182 / 0.227
No. Atoms	Two complexes	Two complexes	One complex
Protein	7824	7953	3923
Peptide	248	252	124
SAH	52	52	26
Solvent	777	933	179
B-factors (Å^2)			
Protein	34.3	29.6	47.3
Peptide	41.4	34.5	42.3
SAH	18.0	16.7	32.0
Solvent	45.2	39.9	46.5
R.m.s. deviations			
Bond lengths (Å)	0.003	0.010	0.004
Bond angles (°)	0.564	0.942	0.683

Values in parenthesis correspond to highest resolution shell. $R_{merge} = \frac{\sum | I - < I > |}{\sum I}$ where I is the observed intensity and $<I>$ is the averaged intensity from multiple observations. $<I / \sigma I>$ indicates the averaged ratio of the intensity (I) to the error of the intensity (σI). $R_{work} = \frac{\sum | F_{observed} - F_{calculated} |}{\sum | F_{observed} |}$ where $F_{observed}$ and $F_{calculated}$ are the observed and calculated structure factors, respectively. R_{free} was calculated using a randomly chosen subset (5%) of reflections that were not used for refinement.

Corresponding author(s): Xiaodong Cheng
Jan E. Carette
Or Gozani

Reporting Summary

Nature Research wishes to improve the reproducibility of the work that we publish. This form provides structure for consistency and transparency in reporting. For further information on Nature Research policies, see Authors & Referees and the Editorial Policy Checklist.

Statistical parameters

When statistical analyses are reported, confirm that the following items are present in the relevant location (e.g. figure legend, table legend, main text, or Methods section).

n/a	Confirmed	
☐	☒	The exact sample size (*n*) for each experimental group/condition, given as a discrete number and unit of measurement
☐	☒	An indication of whether measurements were taken from distinct samples or whether the same sample was measured repeatedly
☐	☒	The statistical test(s) used AND whether they are one- or two-sided *Only common tests should be described solely by name; describe more complex techniques in the Methods section.*
☒	☐	A description of all covariates tested
☐	☒	A description of any assumptions or corrections, such as tests of normality and adjustment for multiple comparisons
☐	☒	A full description of the statistics including central tendency (e.g. means) or other basic estimates (e.g. regression coefficient) AND variation (e.g. standard deviation) or associated estimates of uncertainty (e.g. confidence intervals)
☐	☒	For null hypothesis testing, the test statistic (e.g. *F*, *t*, *r*) with confidence intervals, effect sizes, degrees of freedom and *P* value noted *Give P values as exact values whenever suitable.*
☒	☐	For Bayesian analysis, information on the choice of priors and Markov chain Monte Carlo settings
☒	☐	For hierarchical and complex designs, identification of the appropriate level for tests and full reporting of outcomes
☒	☐	Estimates of effect sizes (e.g. Cohen's *d*, Pearson's *r*), indicating how they were calculated
☐	☒	Clearly defined error bars *State explicitly what error bars represent (e.g. SD, SE, CI)*

Our web collection on statistics for biologists may be useful.

Software and code

Policy information about availability of computer code

Data collection	X-ray collection: HKL2000. Bio-Tek plate readers: Gen5 (v3.04.17). Microscopy: NIS elements (v4.60), Volocity 3D analysis (Perkin Elmer).
Data analysis	Structural analysis: PHENIX PHASER, PHENIX REFINE, and COOT. Statistical analysis: GraphPad Prism 7.0, KaleidaGraph 4.5. Mass spectrometry analysis: MaxQuant (version 1.5.5.1). Image analysis: ImageJ 1.51 (NIH). Pymol (Schrodinger, v2.2). Metabolic analysis: Agilent Masshunter B08. Actin motility: FAST (Fast Automated Spud Trekker) software (Askel et al. Cell Reports, 2015).

For manuscripts utilizing custom algorithms or software that are central to the research but not yet described in published literature, software must be made available to editors/reviewers upon request. We strongly encourage code deposition in a community repository (e.g. GitHub). See the Nature Research guidelines for submitting code & software for further information.

Data

Policy information about availability of data

All manuscripts must include a data availability statement. This statement should provide the following information, where applicable:

- Accession codes, unique identifiers, or web links for publicly available datasets
- A list of figures that have associated raw data
- A description of any restrictions on data availability

The X-ray structures (coordinates and structure factor files) of SETD3 with bound actin peptide have been submitted to PDB under accession number 6MBJ (P21),

6MBK (Two complexes in P212121) and 6MBL (one complex in P212121). Source data for this study are provided as supplementary information (Fig. 4d, 5b, 5e, 5f, 5i, 5k; Extended Data Fig. 7e, 9c, 9h). Source gel data provided for cropped images (Fig. 1a, 1d, 1e, 2a, 2c, 3a-f,g, 4c, 5g, 5j; Extended Data Fig. 1b) is provided in Supplementary Figure 1. Mass spectrometry data associated with Fig. 1c/Extended Data Fig. 1h and Fig. 3i are provided as a Supplementary Tables. Additional requests can be made to the corresponding authors.

Field-specific reporting

Please select the best fit for your research. If you are not sure, read the appropriate sections before making your selection.

☒ Life sciences ☐ Behavioural & social sciences ☐ Ecological, evolutionary & environmental sciences

For a reference copy of the document with all sections, see nature.com/authors/policies/ReportingSummary-flat.pdf

Life sciences study design

All studies must disclose on these points even when the disclosure is negative.

Sample size	No statistical measure was used to predetermine sample size. The dystocia phenotypic analysis resulted in an almost binary outcome leading to a strong conclusion with the sample size provided.
Data exclusions	No data were excluded
Replication	Experiments were replicated as indicated in the figure legends. Generally, all experiments were performed with three independent biological replicates. All results repeated during replication.
Randomization	No randomization was necessary as only single variables changed per experiment
Blinding	Blinding was not necessary as any phenotypic assessment or other measurements was performed using discrete, quantitative measurements

Reporting for specific materials, systems and methods

Materials & experimental systems

n/a	Involved in the study
☐	☒ Unique biological materials
☐	☒ Antibodies
☐	☒ Eukaryotic cell lines
☒	☐ Palaeontology
☐	☒ Animals and other organisms
☒	☐ Human research participants

Methods

n/a	Involved in the study
☒	☐ ChIP-seq
☒	☐ Flow cytometry
☒	☐ MRI-based neuroimaging

Unique biological materials

Policy information about availability of materials

Obtaining unique materials	Most materials are freely commercially available from common sources. Anti-actin-H73(3-me) antibody generated in this study is available upon request.

Antibodies

Antibodies used	Primary: SETD3 (Abcam, #176582, Lot GR283420-5); Actin (Cytoskeleton, #AAN01, Lot 123); Beta-tubulin (Millipore, #05-661 clone AA2, Lot 2834905); H3K4me2 (Cell Signaling, #9725); H3K36me2 (Cell Signaling, #2901); GFP (Invitrogen, A-11122). Anti-actin-H73(3-me) polyclonal antibody was made in-house. Secondary: Alexa488 anti-rabbit antibody (Life Technologies, A-11008), anti-rabbit-HRP (Jackson Immunoresearch, 711-035-152), anti-mouse-HRP (715-035-151)
Validation	SETD3 antibody validated by loss of detection after CRISPR/Cas9 knockout with multiple guide RNAs. Actin, beta-tubulin, and secondary antibodies were validated by the vendor across multiple cell types. Anti-actin-H73(3-me) polyclonal antibody was validated by dot blot with unmodified, H73(3-me), and H73(1-me) peptides and western blotting with cell extracts where actin methylation was quantified by mass spectrometry. H3K36me2 and H3K4me2 antibodies were validated by the vendor and independently on a peptide array containing multiple modified histone peptides.

Eukaryotic cell lines

Policy information about cell lines

Cell line source(s)	HEK293T, H1-Hela, HT1080, and primary uterine smooth muscle cells were all acquired from ATCC. Murine embryonic fibroblasts (MEFs) were generated from mice in this study.
Authentication	HEK293T, H1-Hela, HT1080, and primary uterine smooth muscle cells were authenticated by ATCC. MEFs were genotyped from residual tissue after embryonic dissection and the presence of SETD3 was probed by western blot in this study.
Mycoplasma contamination	Cell lines were declared free of mycoplasma by ATCC. MEFs were not tested.
Commonly misidentified lines (See ICLAC register)	no misidentified lines utilized in this study

Animals and other organisms

Policy information about studies involving animals; ARRIVE guidelines recommended for reporting animal research

Laboratory animals	Mice: Strains derived from C57BL/6N - Setd3tm1.1(NCOM)Mfgc/Tcp heterozygous mice. Timed pregnancy matings were performed with C57BL/6N male mice. Male mice began breeding at 8 weeks and female mice at 6 weeks. Typically, mice no older than 6 months old were used in this study.
Wild animals	No wild animals used
Field-collected samples	No field-collected samples used.